MECHANICAL OPTIMIZATION OF VASCULAR BYPASS GRAFTS

A Thesis
Presented to
The Academic Faculty

By

Luc Felden

In Partial Fulfillment
Of the Requirements for the Degree
Master of Science in Mechanical Engineering

Georgia Institute of Technology
May 2005

MECHANICAL OPTIMIZATION OF VASCULAR BYPASS GRAFTS

Approved by:

Dr. David N. Ku, Advisor
The George W. Woodruff School of Mechanical Engineering
Georgia Institute of Technology

Dr. Alexander Rachev, Co-Advisor
The George W. Woodruff School of Mechanical Engineering
Georgia Institute of Technology

Dr. Elliot L. Chaikof
Department of Surgery
Emory University School of Medicine

Date Approved: March 28, 2005

ACKNOWLEDGEMENTS

I wish to express my genuine gratitude to my advisor Dr. Ku, for offering me an opportunity to work in his lab and for his guidance in my research. I particularly wish to thank Dr. Rachev for his daily assistance on this project. I sincerely thank Dr. Chaikof for his review and comments. I thank you all for your help and friendship along this year.

My heartfelt appreciation goes to all my lab mates from whom I learned more about the American way of life.

I am deeply grateful to my family and friends for the support and love they have provided me while I was abroad.

TABLE OF CONTENTS

LIST OF TABLES

LIST OF FIGURES

LIST OF SYMBOLS or ABBREVIATIONS

CABG:	Coronary artery bypass graft
CCHA:	Canine carotid host artery
EC:	Endothelial cells
Ep:	Peterson modulus (known in the literature as "Pressure-strain elastic modulus", "elastic modulus", "elastance" or "functional stiffness")
ePTFE:	Expanded polythetrafluoroethane or Gore-Tex®
HCHA:	Human coronary host artery
IH:	Intimal hyperplasia
IMA:	Internal mammary artery
IOG:	Ideal optimized graft
LCCA:	Left circumflex coronary artery
PET:	Polyethylene terephthala or Dacron®
PVA:	Poly(Vinyl Alcohol)
RCCA:	Right carotid canine artery
SEF:	Strain Energy Density Function
SMC:	Smooth muscles cells
SVG:	Synthetic vascular graft
TEAG:	Tissue Engineered Arterial Graft
ZSS:	Zero Stress State

SUMMARY

Synthetic vascular grafts are useful to bypass diseased arteries. The long-term failure of synthetic grafts is primarily due to intimal hyperplasia at the anastomotic sites. The accelerated intimal hyperplasia may stem from a compliance mismatch between the host artery and the graft since commercially available synthetic conduits are much stiffer than an artery. The objective of this thesis is to design a method for fabricating a vascular graft that mechanically matches the patient's native artery over the expected physiologic range of pressures. The creation of an optimized mechanical graft will hopefully lead to an improvement in patency rates.

The mechanical equivalency between the graft and the host artery is defined locally by several criteria including the diameter upon inflation, the elasticity at mean pressure, and axial force. A single parameter mathematical model (Strain Energy Density Function with one Invariant) for a thin-walled tube is used to describe of the final mechanical behavior of a synthetic graft. For the general problem, the objective would be to fabricate a mechanics-matching vascular graft for each host artery. Typically, fabrication parameters are set initially and the properties of the fabricated graft are measured. However, by modeling the entire fabrication process and final mechanical properties, it is possible to invert the situation and let the typical output mechanical values be used to define the fabrication parameters. The resultant fabricated graft will then be mechanically matching. As a proof-of-concept, several prototype synthetic grafts were manufactured and characterized by a single Invariant to match a canine artery. The

resultant graft equaled the diameter upon inflation, the elasticity at mean pressure, and axial force of the native canine artery within 6%.

An alternative to making an individual graft for each artery is also presented. A surgeon may choose the best graft from a set of pre-manufactured grafts, using a computer program algorithm for best fit using two parameters in a neighborhood. This method for the optimal graft selection process is demonstrated for a set of six prototype grafts. The design optimization problem was solved for both canine carotid and human coronary arteries.

In conclusion, the overall process of design, fabrication and selection of a mechanics matching synthetic vascular graft is shown to be reliable and robust.

CHAPTER 1

INTRODUCTION

Three million Americans suffer cardiovascular diseases. Atherosclerosis, which is the main cause of cardiovascular diseases, narrows and stiffens the artery. This ultimately leads to the blockage of the artery with a high risk of heart attack and stroke. Bypass surgery is useful to bypass the diseased segments and restore the blood supply to the distal tissues. Almost 500,000 patients per year need a coronary artery bypass grafts (CABG) surgery in the U.S. Today, the patient's veins or arteries are used as CABGs. However, in at least 30% of patients, the autologous conduits can not be used because of pre-existing disease or previous use [7]. Synthetic Vascular Grafts (SVG) would then provide an important alternative while reducing surgery time, recovery time, patient discomfort and complications.

SVG which are currently made of Gore-Tex (PET) or Dacron (ePTFE), are applied with great success for large vessels with high blood flow. Small diameter (<6mm) SVG exhibit a short term failure due to a thrombus formation and a late term failure due a local proliferation of cells that cause an occlusion. Their high occlusion rates make them unacceptable for use as coronary artery bypass grafts (CABG). Therefore, the need of a small diameter SVG remains.

1.1 Atherosclerosis*

Atherosclerosis is one of several types of "arterio"-sclerosis, which is characterized by thickening and stiffening of artery walls, but the two terms are often used to mean the same thing. Atherosclerosis is a condition in which fatty material is deposited along the walls of arteries. This fatty material thickens, stiffens, and may eventually block the arteries. This lesion typically occurs near bifurcations as illustrated in Fig. 1.1.

Atherosclerosis is a common disorder of the arteries. Fat, cholesterol, and other substances accumulate in the walls of arteries and form "atheromas" or plaques. Eventually, this fatty tissue can erode the wall of the artery, diminish its elasticity (stretchiness) and interfere with blood flow. Plaques can also rupture, causing debris to migrate downstream within an artery. This is a common cause of heart attack and stroke. Clots can also form around the plaque deposits, further interfering with blood flow and posing added danger if they break off and travel to the heart, lungs, or brain. Many physicians now suspect that there is an immune system component to the problem (inflammation may help cause atherosclerosis). When blood flow in the arteries to heart muscle becomes severely restricted, it leads to symptoms like chest pain.

---

* *Based on MedlinePlus Medical Encyclopedia: Atherosclerosis*

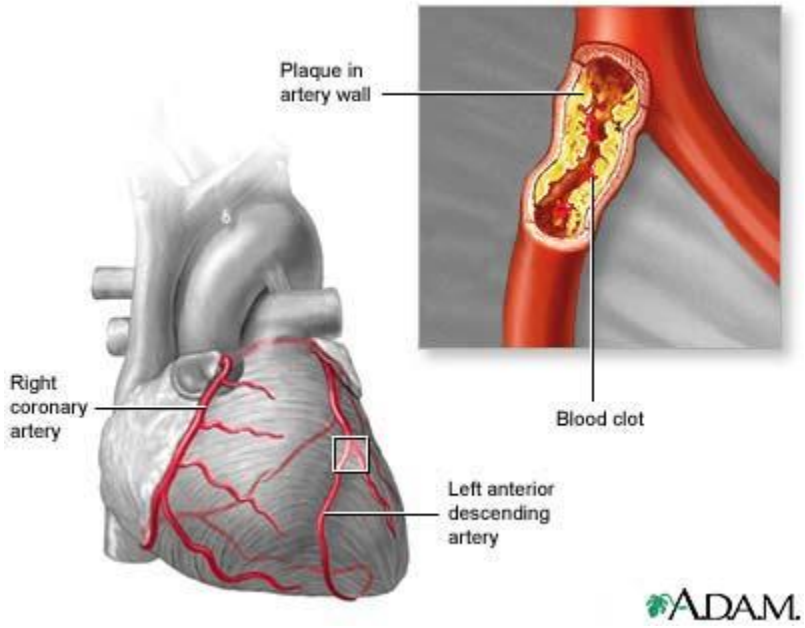

Figure 1.1: Cross section of diseased coronary arteries (ADAM)

1.2 Treatments[†]

Medications (cholestyramine, colestipol, nicotinic acid, …) are usually the first step in treating cardiovascular diseases. Balloon angioplasty uses a balloon-tipped catheter to flatten plaque and increase the blood flow past the deposits. The technique is used to open the arteries of the heart and other arteries in the body. Another widely used technique is stenting, which consists of implanting a small metal device inside the artery (usually following angioplasty) to keep the artery open. Surgically removing deposits (endarterectomy) may be recommended in some cases. The invasive procedure of bypass surgery is reserved to end-stage atherosclerosis. It uses a normal artery or vein from the patient to create a bridge that bypasses the blocked section of the artery. In absence of a

[†] *Based on MedlinePlus Medical Encyclopedia: Atherosclerosis*

good autologous conduit because of pre-existing disease or previous use, synthetic vascular grafts are needed.

1.3 Problems with current grafts

Current synthetic grafts are made of Dacron (PTE) and Gore-Tex (ePTFE). They are predominantly used for aortic/iliac with a relatively good five year patency rate of 80 to 90% [26]. However, their high occlusion rates for diameters less than 6 mm make them unacceptable for use as CABG. The occlusion is either caused by the development of anastomotic intimal hyperplasia (IH) or thrombus formation [42, 56]. The occlusions can be classified into two major areas:

i. Early failure that happenes within 30 days.
ii. Late failure that occurs over 2 months to 2 years.

These patency rates are fairly low compared to the patency rates of autologous conduits. The saphenous vein was reported with a ten year patency rates as high as 77% [30] and the internal mammary artery can maintain its integrity and relative freedom from atherosclerosis with follow up to 20 years [19]. Moreover, synthetics grafts are more involved in infections [26].

The major cause of failure in the short term is typically due to thrombus formation. 90% of thrombosis on vascular grafts occur within 24 hours. Several strategies have been pursued to prevent thrombosis. One is to seed endothelial cells (ECs) on the luminal surface of the synthetic graft. Indeed, ECs prevent blood-borne platelet aggregations that usually cause the thrombosis. Several studies have demonstrated the ability to seed ECs on PTFE grafts [22]. Another technique is to present bioactive

molecules at the surface of the graft. The active agent can be presented by elution, attachment or bonding [27, 28]. The result is a local reduction of thrombosis [24].

The long term failure is primarily due to the proliferation of smooth muscles cells (SMCs) and fibroblasts at the anastomotic sites [21]. This cellular lesion is called Intima Hyperplasia (IH). The resultant hyperplasia appears to be greatest at the downstream or distal anastomosis and is dependent on the graft material [48]. Physical forces are also involved in the formation and development of IH. An overview of the mechanisms resulting in the formation of IH reported in the literature is given in the next section.

1.4 Theories on Intimal Hyperplasia

IH may be an adaptative response with the remodeling of the media rather than an inflammatory response as white blood cells and monocytes are very rare in this lesion [15]. Many research groups were studying the possible mechanism resulting in formation of IH. Three stimuli are widely tested and reported in the literature:

i. a low wall shear stress
ii. a high solid mechanics stress
iii. a mismatch in compliance and geometry

They are all related to mechanics-mismatch between the graft and the host artery.

Wall shear stress

There is a widespread belief that low wall shear stress promotes the formation of IH [36, 37, 46; 49]. The intimal thickness appears to be strongly correlated to the inverse of the WSS as shown in Fig. 1.2. [26]. Arteries do not suffer from this low WSS because they adapt their diameter to maintain a relatively constant WSS. Synthetic grafts can not do this and are stiffer than native arteries as shown in Fig 1.3.

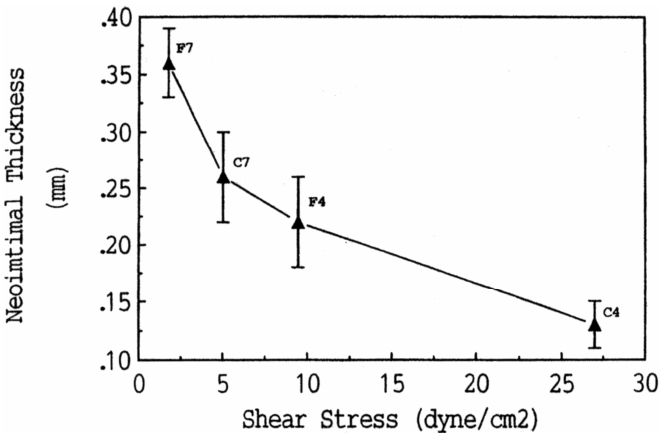

Figure 1.2: Graph of the anastomotic neointima thickness (mean ± SEM) in relation to shear stress at the anastomosis [49]
F: femoral grafts, C: carotid grafts; 4:4 mm end; &:7 mm end

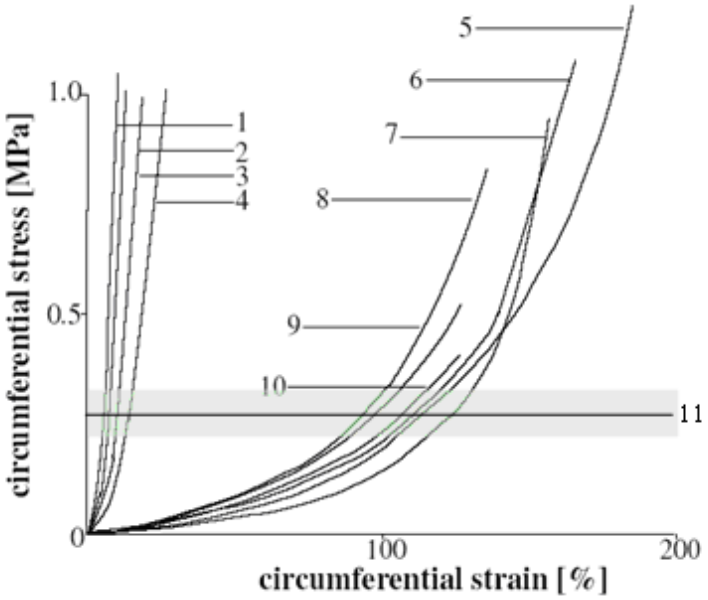

Figure 1.3: Circumferential stress strain relationship of several vascular prostheses and arterial tissues in circumferential direction [41]
, 1: PET woven; 2: PTFE woven; 3: PET knitted; 4: PTFE knitted; 5: iliac artery; 6: distal abdominal aorta; 7: femoral artery; 8: proximal abdominal aorta; 9: distal thoracic aorta; 10: proximal thoracic aorta, 11: Approximated mean circumferential stress [54]

Thus, any perturbation that creates low shear stress in the anastomotic sites will contribute to the formation of IH which leads to the occlusion of the graft. Because the WSS is proportional to the inverse of the diameter to the third power, the graft must be sized correctly. The shape and angle of the anastomotic junction for an end-to-side graft are very important. An unadapted angle may create vortices, returning or stagnating flow which would decrease locally the WSS, as illustrated in Fig. 1.4. For an end-to-end graft flow disturbances are induced by a lack of compliance of the graft.

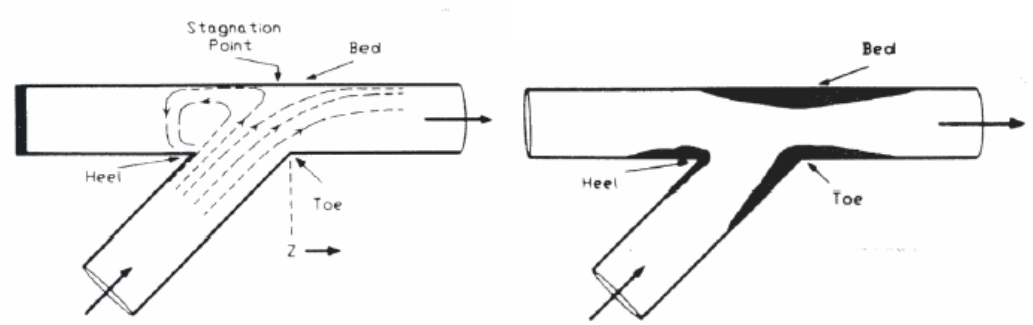

Figure 1.4: Particle deposit at the anastomosis [48]

High solid mechanics stress

Solid mechanics stress in the arterial wall contributes also to the formation and development of IH [11]. The thickening of the intima is observed at the anastomosis when low compliance grafts are used [9; 12]. The graft stiffness causes the arterial wall to bend as shown in Fig. 1.5.

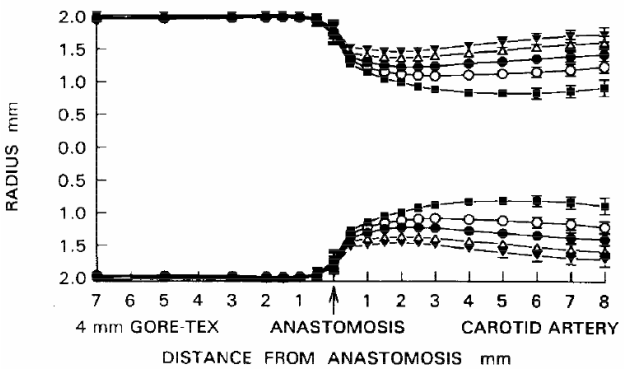

Figure 1.5: Diameter isobars for 18 arteries anastomosed to 4 mm PTFE grafts [10]
, (■) 0 mmHg, (○) 25 mmHg, (♦) 50 mmHg, (△) 100 mmHg, (▼) 200 mmHg

The result of this bending is an increase of the axial and circumferential stresses at the anastomotic sites [32, 43]. The thickening in this area may be an adaptative response of SMC. It has been demonstrated that SMC produce EC and replicate when they are subjected to high levels of distension and tangential stress [48]. The production of EC and replication of SMC increases the amount of load bearing material and tends to maintain a uniform wall stress along the artery.

Compliance and geometrical mismatch

The concept of compliance (C) has been introduced to simplify the clinical approach to a very complex physical phenomenon [48]. Compliance is the mechanical property of a tube that expresses a change of diameter with respect to a change of pressure, as follows

$$C = \frac{\Delta D}{\Delta P}\frac{1}{D} \tag{1.1}$$

where D is the diameter of the tube, and ΔD is the change of diameter with respect to the change of pressure. For a fixed deformed state, the compliance depends on the current

diameter/thickness ratio and on the incremental elastic modulus of the material of the tube. Thus, the compliance is a local descriptor of the vessel deformability around a fixed deformed state.

The compliance mismatch between the graft and the host artery involves both low WSS and high solid mechanic stress mechanisms that promote the formation and development of IH. Some groups placed grafts of equivalent size and different compliance to identify the correlation between compliance mismatch and the formation of IH. An interpretation is that as compliance mismatch increases, patency decreases, as shown in Fig. 1.6 [1, 48; 58].

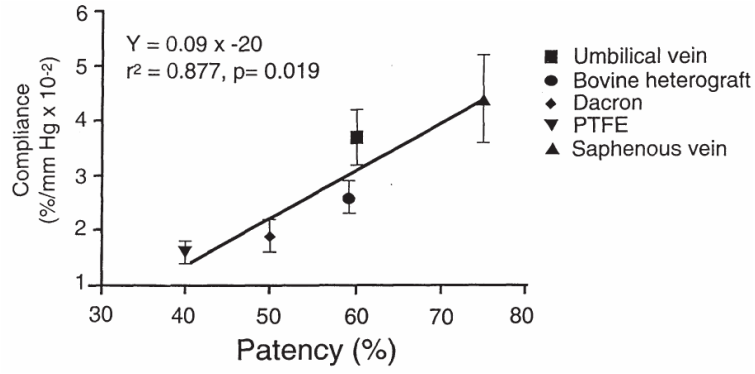

Figure 1.6: Data reported from compliance of various biological and prosthetic grafts versus patency rate [48]

This result is concordant with the finding that autologous grafts, which have compliance more like the host artery, have better patency rates than synthetic grafts. Compliance mismatch is also related to other mechanisms that leads to vibratory weakening of the arterial wall, loss of EC viability and anastomosed aneurysm [14]. Today, it is a widespread belief that the mechanics mismatch caused by the difference in the

mechanical response of the graft and the host artery under physiological condition promote the formation and progression of IH. This mechanical matching is not possible over the physiologic range of pressure for Dacron and Gore-Tex grafts. A graft whose diameter matches the diameter of the host artery can easily be selected to normalize the mean shear stress. However, due to the high stiffness of these grafts, the matching can not occur for all deformed geometry of the artery during the cardiac circle.

1.5 Hypothesis

The hypothesis of this thesis is that a mechanics matching graft with biocompatibility, hydrophilicity, and geometric matching can be designed and fabricated to reduce intimal hyperplasia.

1.6 Objectives

The goals of this project are:

i. To specify and design a mechanical matching vascular graft,
ii. To build an example graft prototype,
iii. To verify the mechanical properties of the graft prototype,
iv. Create an algorithm to select a matching graft from a set of grafts.

CHAPTER 2

EXPERIMENTAL DESIGN AND METHODS

2.1 Design concept

A mathematical model (Section 2.3) based on the finite inflation and extension of a cylindrical thin wall tube made of an elastic material (with a SEF) is used to describe the end-to-end anastomosed graft. The mechanical equivalency between the graft and the host artery is defined mathematically by a criterion (Section 2.2). The model incorporates parameters usable for manufacturing a graft. Therefore, by solving the inverse inflation of an elastic tube that verifies the criterion, the fabrication parameters can be found. This procedure is called "design optimization" (Section 2.4.1).

Before being able to apply the design optimization, the SEF in terms of material constants must be determined (Section 2.4.2 & 2.4.3). This determination is made by performing a typical pressure diameter experiment (Section 2.6) on a tube made of elastic material.

2.2 Specification of mechanics-matching grafts

The specification of a mechanics-matching graft is needed to define the deformed state of a matching graft and to apply the design optimization (Section 2.3.1) to find its fabrication parameters.

Mechanically equivalency

The graft is mechanically equivalent to its host artery at a given pressure when their pressure-diameter curves are tangent and the axial force is restored. This is equivalent to say that for a given pressure, the slope of the pressure diameter curves, the diameters and the axial forces are the same for the graft and the host artery.

Mechanics matching criterion

The chosen criterion of mechanics matching requires that the mechanically equivalency occurs at the mean pressure. In the following this criterion is called the "one-point" criterion. As the Peterson modulus is equal to the slope of the pressure diameter curve multiplied by the mean diameter, the one point criterion is written as follows

$$r_{iam} = r_i\,,\ E_{pam} = E_{pgm}\,,\ F_{zam} = F_{zgm}\,, \tag{2.1}$$

where r_i is the deformed radius of the graft, r_{iam} is the deformed diameter of the artery at the mean pressure, E_p is the Peterson modulus, F_z is the axial force, and the subscripts a and g stand for artery and graft and m stands for value at the mean pressure.

2.3 Mathematical model

The mathematical model (inflation and extension of thin-wall tube) is needed because it includes the fabrication parameters which are found by applying the design optimization (Section 2.3.1).

Modeling includes: i) assumptions about the vessel geometry (geometrical model); ii) assumptions about the interaction of the vessel with other bodies (model of applied loads and boundary condition); iii) mathematical description of the mechanical properties of the material (selection of constitutive equations); and iv) modeling of the

deformation process by introducing hypotheses for the character of the stress and/or strain. [44]

The graft has a geometry that can be considered as tubular. In order to simplify the model, the following conditions are assumed:

i. The geometry is considered to be a thin cylindrical membrane of constant thickness (a circular membrane is a geometrical object where the thickness h is much smaller than the longitudinal length l and the radius r. A common criterion is $\frac{r}{h} > 5$)

ii. The loadings (internal pressure and longitudinal extension) are axisymetric and quasi-static.

Condition (i) implies that the circumferential stress $\vec{\sigma}_\theta$ and the longitudinal stress $\vec{\sigma}_z$ are uniformly distributed across the thickness and that the radial stress $\vec{\sigma}_r$ is null everywhere across the membrane thickness as illustrated in Fig. 2.1

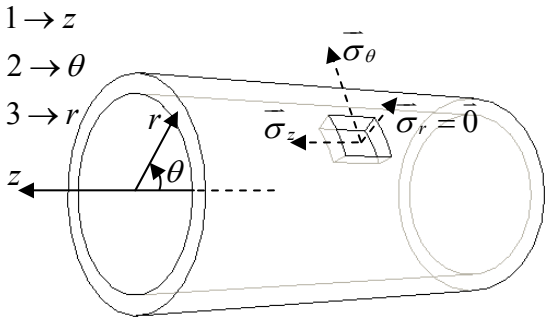

Figure 2.1: Principal directions and stress components in a cylindrical membrane (in cylindrical polar coordinates)

Kinematics and finite elasticity

The deformed position $\vec{x}$ of a body is related to its undeformed position $\vec{X}$ by the deformation tensor

$$\underset{\sim}{F} = \frac{\partial \vec{x}}{\partial \vec{X}}, \tag{2.2}$$

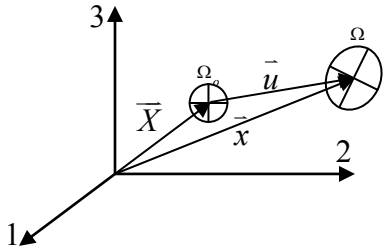

Figure 2.2: Current and reference position

The principal stretches λ_i of the deformation are determined by taking the square root of the eigenvalues of the right Cauchy-Green tensor

$$\underset{\sim}{C} = \underset{\sim}{F}^T \underset{\sim}{F}, \tag{2.3}$$

The stresses of an elastic material can be derived from a SEF W that is a function of the strain invariant of $\underset{\sim}{C}$. For an isotropic material

$$W = W\left(I_1, I_2, I_3\right), \tag{2.4}$$

where

$$I_1 = tr\underset{\sim}{C} = \lambda_1^2 + \lambda_2^2 + \lambda_3^2, \tag{2.5}$$

$$I_2 = \frac{1}{2}\left[\left(tr\underset{\sim}{C}\right)^2 - tr\left(\underset{\sim}{C}\right)^2\right] = \lambda_1^2\lambda_2^2 + \lambda_2^2\lambda_3^2 + \lambda_3^2\lambda_1^2,$$

$$I_3 = \det \underset{\sim}{C} = \lambda_1^2\lambda_2^2\lambda_3^2,$$

$\sqrt{I_3}$ characterizes the change of volume. When the material is incompressible $I_3 = 1$, and consequently the SEF is only a function of I_1, I_2 and the stretch ratios are not independent

$$\lambda_1 \lambda_2 \lambda_3 = 1 \tag{2.6}$$

The Cauchy stress for an elastic isotropic incompressible material is given by

$$\sigma_i = \lambda_i^2 \frac{\partial W}{\partial E_i} + p, \; i = 1,2,3, \tag{2.7}$$

where p is an unknown scalar function which appears due to the material incompressibility. The E_i are the principal components of the Green tensor

$$E_i = \frac{1}{2}\left(\lambda_i^2 - 1\right), \; i = 1,2,3, \tag{2.8}$$

The unloaded configuration Ω_o of the graft corresponds to the zero stress state configuration (Fig. 2.3). This is demonstrated by the observation that a graft segment is kept in position when cut radially.

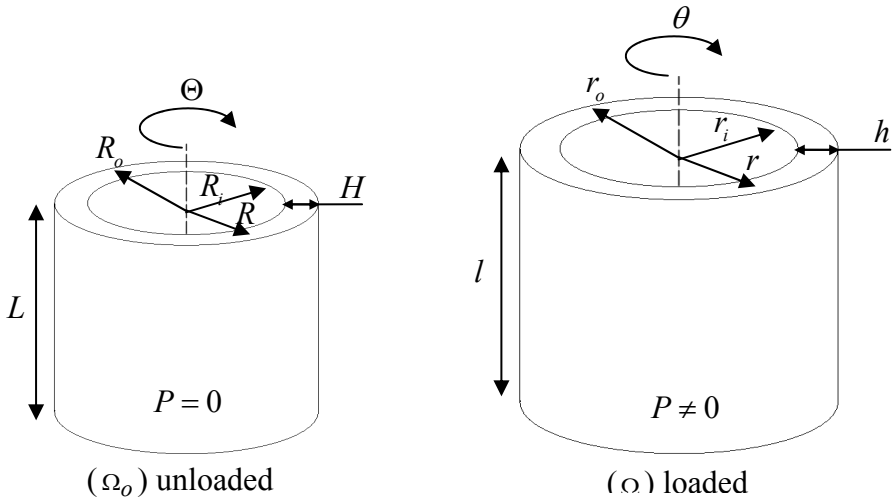

Figure 2.3: Unloaded and loaded configurations

By denoting the cylindrical coordinates before and after deformation by (R,Θ,Z) and (r,θ,z), the stretch ratios in the axial, circumferential, and radial are

$$\lambda_z = \frac{l}{L},\ \lambda_\theta = \frac{r}{R},\ \lambda_r = \frac{h}{H} \tag{2.9}$$

Equilibrium

Condition (ii) implies that the theory of static mechanics is applicable to derive the membrane stresses. In absence of body forces, the equilibrium equation is deduced from the overall free-body diagram (Fig. 2.4) in the radial direction

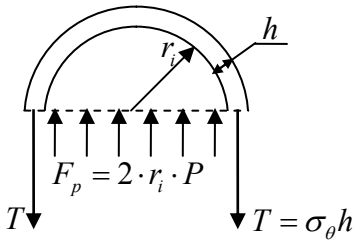

Figure 2.4: Free body diagram of the cylindrical membrane in the radial direction

The equation arising from the equilibrium $F_p = 2T$ is known as the *law of Laplace*

$$\sigma_\theta = \frac{Pr_i}{h}, \tag{2.10}$$

where P is the internal pressure, r_i the inner diameter and h the thickness of the membrane. It follows that when all loads are removed, i.e. $P = 0$, the tube is in the zero stress state.

Constitutive equations

It follows from the condition of incompressibility (Eq. (2.6)) that I_1 and I_2 are only a function of λ_1 and λ_2, and

$$\lambda_r = \frac{1}{\lambda_z \lambda_\pi},\ h = \frac{H}{\lambda_z \lambda_\theta}, \tag{2.11}$$

Given Eq. (2.8), the SEF in Eq. (2.7) is only a function of E_z and E_θ. Given the membrane assumption that reduces the radial stress $\bar{\sigma}_r$ to zero everywhere, the constitutive equations are

$$\sigma_z = \lambda_z^2 \frac{\partial W}{\partial E_z},\ \sigma_\theta = \lambda_\theta^2 \frac{\partial W}{\partial E_\theta}, \tag{2.12}$$

where $W = W\left(E_z, E_\theta\right)$. The axial and circumferential stress are obviously functions of λ_z and λ_θ.

Using the Eqs. (2.9), (2.11), and (2.12), the *law of Laplace* takes the form

$$\sigma_\theta\left(\lambda_\theta\right) = P\left(\frac{R\lambda_\theta^2 \lambda_z}{H} - \frac{1}{2}\right), \tag{2.13}$$

The model is used in a *direct approach*. Given the input, i.e. the pressure, and the model, the output is determined as illustrated in Fig. 2.5

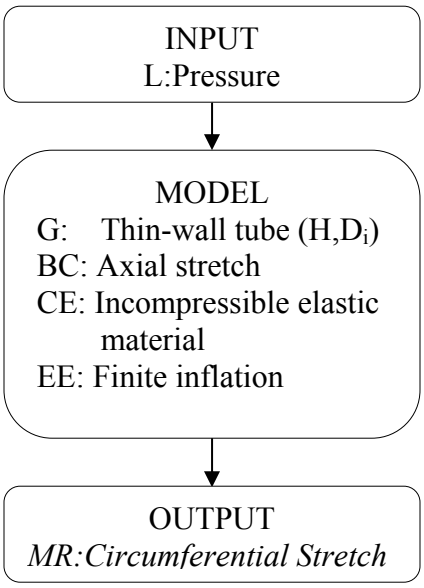

Figure 2.5: Representation of the model *(direct approach)*
(L: Load, G: Geometry, BC: Boundary Condition, CE: Constitutive Equation, EE: Evolution Equation)

The Peterson modulus and the axial force can also be determined. The Peterson modulus is defined as

$$E_p = \frac{\Delta P}{\Delta r_i} r_i, \tag{2.14}$$

where r_i is the inner radius at the mean prescribed pressure P and ΔP is the difference between the systolic and diastolic pressure and Δr_i is the resulting change of inner radius around the inner radius r_i. As P and r_i depend only on λ_θ, the local Peterson modulus is calculated using the chain rule as follows

$$E_p = \frac{\Delta P}{\Delta \lambda_\theta} \left(\frac{\Delta r_i}{\Delta \lambda_\theta} \right)^{-1} r_i, \tag{2.15}$$

In order to determine the Peterson modulus, Eq. (2.13) is solved for the following pressure

$$P_d = P - \frac{\Delta P}{2}\,, \tag{2.16}$$

$$P = \text{Prescribed Pressure}\,, \tag{2.17}$$

$$P_s = P + \frac{\Delta P}{2}\,, \tag{2.18}$$

Given the Eqs. (2.11) and (2.13), the only unknown of the Peterson modulus E_p is the circumferential stretch ratio λ_θ.

The axial force is determined from

$$F_z = \pi dh\sigma_z \tag{2.19}$$

Given Eqs. (2.9), (2.11), and (2.12), the only unknown parameter for the axial force F_z is the circumferential stretch ratio λ_θ.

In conclusion, given the unloaded configuration Ω_o, the SEF, the axial stretch ratio λ_z, and the applied pressure, the stretch ratio λ_θ is determined and the mechanical responses like the stresses, strains, Peterson modulus or axial force can be calculated. Equation (2.13) is solved numerically using Maple (Appendix A).

2.4 Design

2.4.1 Design optimization

The design optimization solves the inverse problem of finite inflation and extension of a thin wall tube (mathematical model) which verifies the mechanics matching criterion ("one-point criterion). It returns the fabrication parameters needed to build a mechanics matching graft.

Given the Eqs. (2.14) and (2.19), the "one-point" criterion becomes

$$r_{iam} = r_i,\ E_{pam} = \frac{dP_m}{dr_i} r_i,\ F_{zam} = \pi dh\sigma_z, \tag{2.20}$$

The equations relating the deformed dimensions h, r_i of the graft to the initial dimensions R_i, H, stretch ratios $\lambda_z, \lambda_\theta$ and the SEF were already derived. The circumferential stretch ratio λ_θ is an unknown too because the deformed state of the graft is not known. The problem of finite inflation and extension of the graft is not solvable yet because there are four unknown and only tree independent equations. Using the equilibrium condition given by Eq. (2.10) (Law of Laplace), the inverse problem of inflation and extension of the graft reduces to solve the system of four equations given by Eqs. (2.10) and (2.20) in order to determine the four unknowns $R_i, H, \lambda_z, \lambda_\theta$, as illustrated in Fig. 2.6. A Maple program is made to solve this non-linear system (Appendix B).

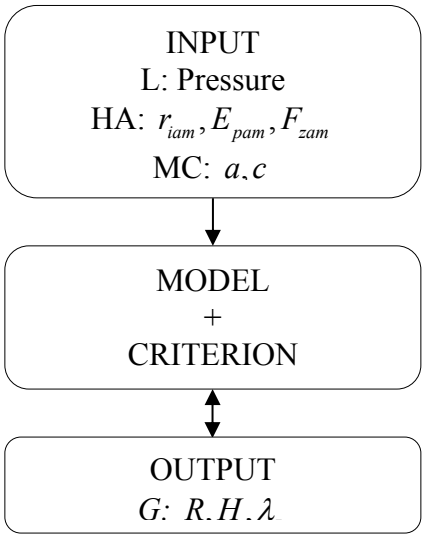

Figure 2.6: Representation of the optimization process
(L: Load, G: Geometry and axial stretch ratio of the graft, HA: Host Artery parameters, MC: PVA hydrogel material constant)

2.4.2 Material requirements

An ideal vascular graft would (1) be biocompatible, (2) be non thrombogenic, (3) have long-term potency, (4) be durable yet compliant, (5) be infection resistant, and (6) be technically facile [26]. All of these requirements are related to the graft material.

To design a compliant graft (4), a biomaterial with soft tissue-like elasticity should be considered.

Moreover its SEF must be known in order to permit the design optimization to be applied. For some elastic biomaterials, such as elastomers (Polyurethanes, Silicon, PVA hydrogel) or other rubber-like materials, the SEF depends solely on the first strain invariant [3, 62], i.e. $W=W(I_1)$. A SEF of this form can easily be determined by uniaxial or biaxial tests.

A tube made of a particular material must be able to verify the "one-point" criterion with dimensions easy to manufacture (6). A compliant graft must at least verify the following:

$$E_{pg} = E_{pa}, \tag{2.21}$$

$$r_g = r_a, \tag{2.22}$$

where subscript "a" refers to the host artery (Table 2.1) and subscript "g" refers to the graft (Table 2.2). The functional stiffness E_p [40] is related to the structural stiffness E (Young's modulus) by the approximation [16]:

$$E_p \approx E\frac{h}{r} \tag{2.23}$$

where r and h are respectively the radius and thickness of the cylinder that represent the graft or the host artery. Using (2.1), (2.2) and (2.3) the possible thickness of the graft by solving

$$h_g = \frac{E_{pa} r_a}{E_g} \tag{2.24}$$

The value of the thickness demonstrates whether or not the material can be used for fabricating a compliant graft if correctly processed and designed.

Table 2.1: Mechanical properties of a canine coronary artery [16]

P [mmHg]	r [mm]	h [mm]	E_p [kPa]
102	1.58	0.13	149

P: mean pressure, r: radius, h: thickness, E_p: Peterson modulus

Current graft

The possibility of manufacturing will be checked for current synthetic grafts, whose mechanical properties are given in table 2.1.

Table 2.2: Mechanical properties of current synthetic grafts (Goodfellow Corporation, Gore & Associates Inc)

	E [MPa]	σ_{ult} [MPa]
Dacron (PET)	2000	80
Gore-Tex (ePTFE)	400	14

E: Young's modulus, σ_{ult}: Ultimate strength

PVA hydrogel

The manufacturing ease will also be verified for PVA hydrogel. This hydrogel can be fabricated to exhibit a Young's modulus between 0.36 MPa and 1.01 MPa [59].

2.4.3 Identification of the SEF of a particular form $W=W(I_1)$

Generally, data from uniaxial tests (Dumbbell-shaped strips or ring tests, as shown in Fig. 2.7) are sufficient to identify SEF of material belonging to the class $W = W(I_1)$ [13, 45]. The material properties of the graft may depend on the manufacturing process. Then the identification of the SEF is more realistic by inflating a manufactured graft. In this study, the design optimization outcomes include the longitudinal stretch ratio to prevent any buckling or over stretching of the graft. Therefore the formulation of the SEF must be determined and checked in the $\lambda_z \geq 1$ and $\lambda_\theta \geq 1$ domains, as illustrated in Fig 2.7.

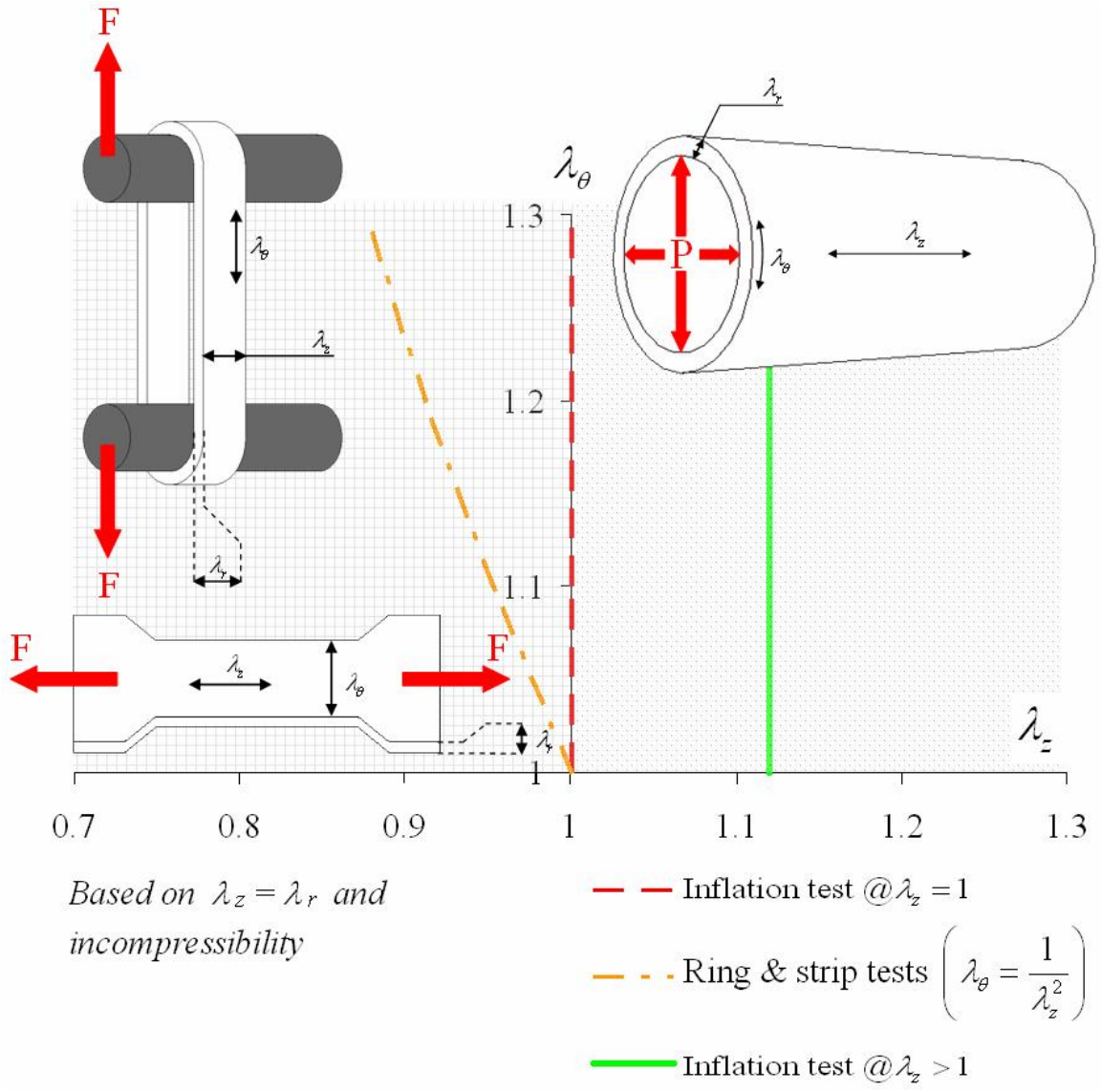

Figure 2.7: Typical identification of $W=W(I_1)$ (squared area) and recommended identification and verification for a graft (dotted area)

The SEF is determined by using the model in an *indirect approach*. Given the input, i.e. the pressure, and the output, i.e. the circumferential stretch ratio, the model is fully described as illustrated in Fig. 2.8

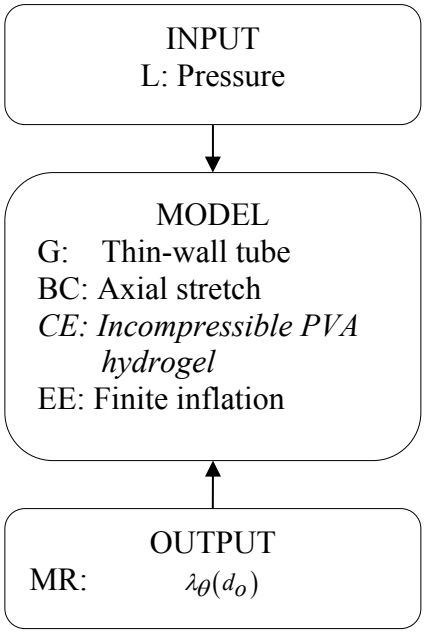

Figure 2.8: Representation of the model *(indirect approach)*
(L: Load, G: Geometry, BC: Boundary Condition, CE: Constitutive Equation, EE: Evolution Equation)

Input and output of the model must be measurable physical values, i.e. forces or displacements. That is why it is necessary to link the circumferential stretch ratio to the measurable outer diameter. Using the condition of incompressibility on a graft segment it follows

$$\pi\left(d_o^2 - d_i^2\right)l = \pi\left(D_o^2 - D_i^2\right)L \tag{2.25}$$

$$d_i = \sqrt{d_o^2 - \frac{D_o^2 - D_i^2}{\lambda_z}} \tag{2.26}$$

$$h = d_o - d_i \tag{2.27}$$

$$d = d_o - h \tag{2.28}$$

Given Eqs. (2.26) to (2.28), the circumferential stretch ratio λ_θ is only a function of d_o. Using the chain rule the derivative of the SEF in Eq. (2.12) is derived as follows

$$\frac{\partial W}{\partial I_1} = \frac{\sigma_\theta}{2\left(\lambda_\theta^2 - \frac{1}{\lambda_z^2 \lambda_\theta^2}\right)}, \tag{2.29}$$

Making use of Eq. (2.13), the set of recorded data $\{P_i, d_{oi}\}$ are transformed into a set of experimental stress-stretch data $\{\sigma_i, \lambda_{\theta i}\}$ that are converted into $\left\{\left(\frac{\partial W}{\partial I_1}\right)_i, I_{1i}\right\}$. Then either a relation between $\frac{\partial W}{\partial I_1}$ and I_1 is known or a reasonable form should be assumed as follows $\frac{\partial W}{\partial I_1} = F(I_1)$. The unknown coefficients are determined by applying the least square method.

2.4.4 Example of first invariant, biocompatible, hydrophilic material

PVA hydrogel is a synthetic hydrogel that combines properties such as biocompatibility, hydrophilicity, and permeability makes them advantageous for use in biomedical applications [25].

PVA hydrogel is a hyperelastic, incompressible, and homogenous (isotropic) solid, which has a SEF that is an exponential function of the first strain invariant I_1 of the right Cauchy-Green tensor

$$W(I_1) = \frac{c}{a}\left[\exp\left[a(I_1 - 3)\right] - 1\right], \tag{2.30}$$

where a and c are material constants [13, 45]. The SEF fully describes the elastic mechanical properties of the material and determines the general 3D stress-strain constitutive relations.

2.4.5 Example of host artery parameters

The design optimization will be tried for a canine carotid host artery and a human coronary host artery. The mechanical response of these arteries is taken from the literature.

Canine carotid host artery

Takamizawa et al. identified a strain energy density function for canine carotid arteries. The vessel dimensions at physiological condition (100 mmHg, in vivo axial length) are given in Table 2.10.

Table 2.3: Vessel dimensions and circumferential stretch ratio at physiological condition ($100 mmHg, \lambda_z = 1.61 \pm 0.17$) [54]

d_o [mm]	d_i [mm]	λ_θ [-]
4.557 ± 0.573	4.093 ± 0.539	1.571 ± 0.097

Data are given as mean ± S.D., n=8

The exponential formulation of the SEF is the following

$$W = C\left(\exp\psi - 1\right), \tag{2.31}$$

Where $\psi = \frac{1}{2}\left(a_{\theta\theta}E_{\theta}^{2} + 2a_{\theta z}E_{\theta}E_{z} + a_{zz}E_{z}^{2}\right)$ and C and the a_{ij} are the material constants, the E is the Green's strain. The material constants assuming zero stress under no load condition (zero initial stress hypothesis) are given in Table 2.11.

Table 2.4: Material constants of the canine carotid artery assuming zero stress under no load condition [54]

C	$a_{\theta\theta}$	$a_{\theta z}$	a_{zz}
[kPa]	[-]	[-]	[-]
17.478	1.3000	0.1061	1.6604
12.965	0.5211	0.1205	0.7345

Data are given as mean (upper) and S.D. (lower row; n=7)

The model of inflation of a thin wall tube described in section 2.2.1 is used to calculate the mechanical responses of the canine carotid arteries because the geometry is a thin cylindrical membrane of constant thickness ($\frac{r}{h} \approx 9.3 > 5$). The Maple code (Appendix A) is used to determine the mechanical responses for the canine carotid artery (Table 2.12). The SEF in the code must be replaced by the SEF of the CCHA given by Eq. (2.31).

Table 2.5: Mechanical responses of the CCHA calculated from the membrane model

P [mmHg]	d_{ia} [mm]	E_{pa} [kPa]	F_{za} [g]
0	2.177	7.7	31.7
20	2.855	13.1	33.4
40	3.344	22.1	37.0
60	3.684	34.5	41.6
80	3.929	49.6	46.6
100	4.115	67.0	51.8
120	4.262	86.1	57.0
140	4.382	106.8	62.2
160	4.483	128.9	67.4
180	4.569	152.0	72.6
200	4.644	176.3	77.8
220	4.710	201.4	82.9
240	4.769	227.4	87.9

P: pressure; d_{ia}: inner diameter; E_{pa}: Peterson modulus; F_{za}: axial force

Human coronary host artery

Data on postmortem human coronary arteries from a healthy 40 year old man are shown in Table 2.14 [16].

Table 2.6: Human LCCA mechanical response [16]

r_i [mm]	h [mm]	E_p [kPa]
2.156	0.644	472

R_i: mean inner radius, h: wall thickness, E_p: Peterson modulus

The mechanical response at the mean pressure is not entirely defined, as the axial force F_z is missing. The design outcomes will be calculated for two different possible axial forces that are 5g, and 50g.

2.5 Building elastic tubes

The elastic tubes are fabricated by injecting the elastic material into tubular molds [8], as illustrated in Fig.2.9. The process to solidify the tube follows the method described in [25].

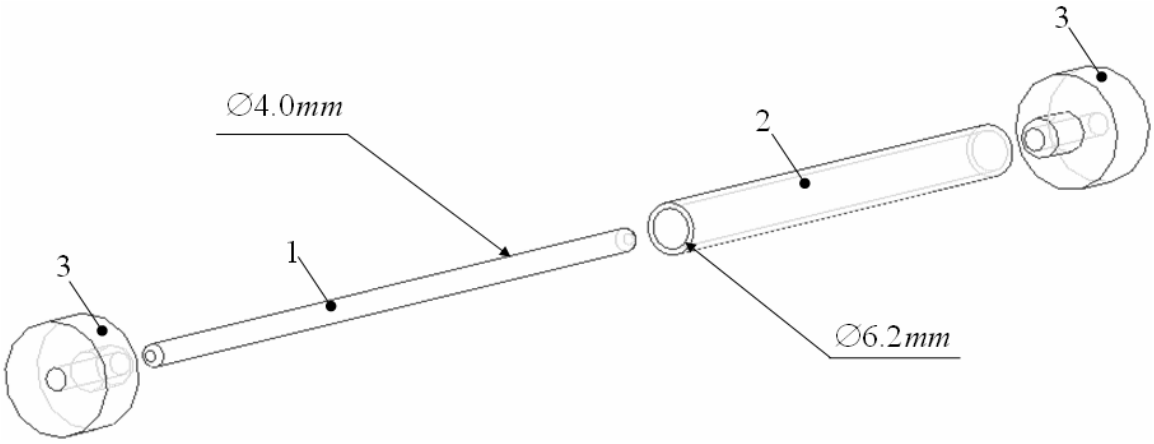

Figure 2.9: Three parts mold to make the tubular graft
(1. Inner stainless steel rod; 2. Outer stainless steel cylinder; 3. Nylon screw fittings to center and maintain the 1. within 2.)

2.6 Identification and verification tests

The mechanical responses of the elastic tube and graft prototype are determined experimentally by pressure-outer diameter measurements. It takes an important place in the design and validation of a mechanics matching graft because

i. The design optimization uses the SEF of the material which is determined by experimentation,

ii. The mathematical model is validated by predicting the inflation of a tube longitudinally stretched,

iii. The pressure diameter response of a graft prototype is compared to its theoretical response to observe the design and fabrication process robustness.

2.6.1 Sample placement

A 30 mm length segment of elastic tube is cut and mounted in the vessel chamber on two stainless steel tubes that matches the lumen of the graft. Both ends of the graft are attached to the stainless steel tubes using strings and usual nodes in order to prevent any leakage. All air bubbles are removed from the flow loop by making the liquid flow to the reservoir, where bubbles can escape.

2.6.2 Initial inner diameter measurement

After all experiments are over, a ring of material located at the middle of the tube sample (where the "cross-section" measurement is made) is cut to identify the inner diameter and wall thickness at the undeformed state. The inner diameter is measured using a CCD video camera (Philips PCVC740K ToUcam Pro) and a video measurement software (AviMéca 2.7.30). A scale is also captured to take the calibration of the measurement. The geometry of the ring is not perfect due to the imperfection of processing, and roughness of the material. Thus the diameter must result from the measure of a set of points $M_i(x_i, y_i)$. The center of the circle is not known, but its position is estimated by the point $Mo(x_o, y_o)$. The measured radius is $r_i = \sqrt{(x_i - x_o)^2 + (y_i - y_o)^2}$, assuming that the measured geometry is a circle. The

average diameter, i.e. the diameter that best fit the real diameter, is obtained by minimizing the Euclidian distance

$$e = \sum \left(r_{th} - r_i \right)^2 , \tag{2.32}$$

where e is the sum of the squared errors, r_{th} is the expected radius, r_i is the measured radius at the point M_i (Fig. 2.10).

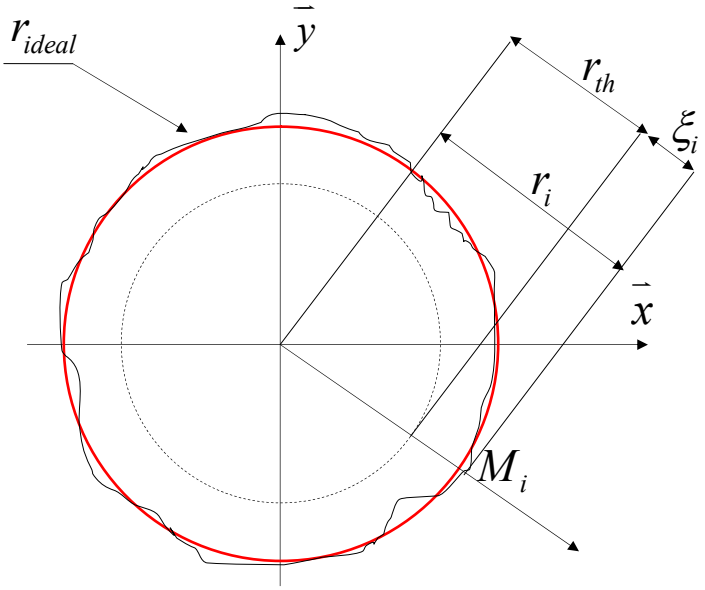

Figure 2.10: Real (solid line) and average (solid red line) radius

2.6.3 Preconditioning

A preliminary study indicates that a three time preconditioning is necessary to reach repeatable loading and unloading curves. Then, before starting the measurement, a preconditioning is made by increasing and decreasing the pressure from 0 mmHg to 400 mmHg at 1 mmHg/s for 3 cycles.

2.6.4 Pressure-outer diameter measurements

Two measurement techniques (“cross-section” and “volume" measurements) are tested to find the most accurate.

Testing method and experimental conditions

Medium: The reservoir and the vessel chamber are initially filled with water at 37°C,

Loads: Quasi static inflation (≈1 mmHg/s) test under constant axial length,

Measures: Each 20 mmHg from 0 mmHg to 400mmHg (3 times)

Cross section

The experimental setup used to measure locally the diameter of the tubes is schematically presented in Fig. 2.11. Pressure is applied to the graft by compressing four 10cc syringes using an Infusion/Withdrawal Syringe Pump (Harvard Apparatus). The pressurization is controlled by both the syringe pump and the clamp located downstream the graft. A pressure transducer (Harvard Apparatus) is immediately connected after the graft but before the clamp for monitoring pressure. The digital display of the pressure is set under the transparent vessel chamber. The pressure digital display and the graft are then filmed at the same time (Fig. 2.11: 10) by a CCD video camera (Philips PCVC740K ToUcam Pro) and recorded on a computer (Acer Aspire 1350 LMi). The diameter is measured using a video measurement software (AviMéca 2.7.30), as illustrated in Fig. 2.12. A scale (Fig. 2.11: 2) allows calibrating the video measurement system.

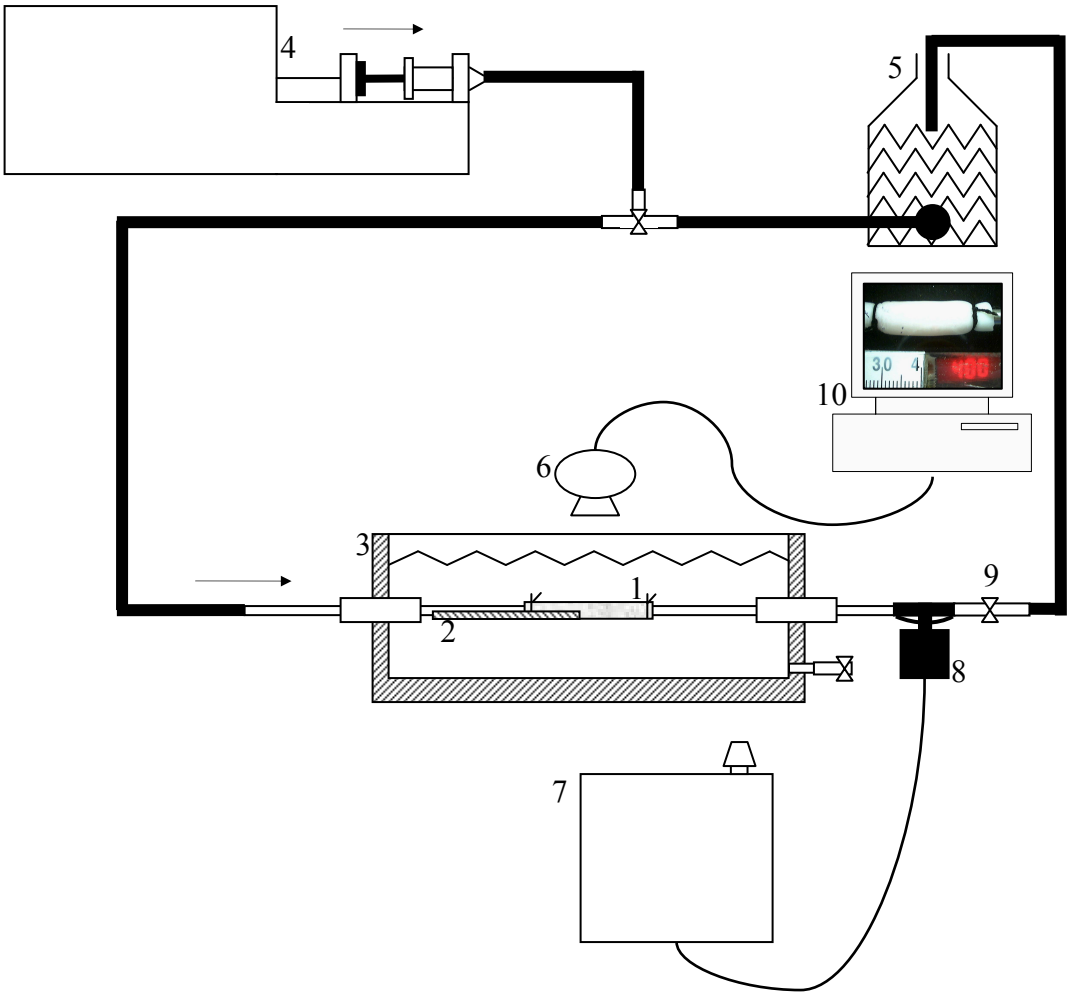

Figure 2.11: Local diameter measurement experimental setup , 1: PVA hydrogel graft sample, 2: Scale, 3: Transparent vessel chamber, 4: Infusion/Withdrawal Syringe Pump (Harvard Apparatus), 5: Reservoir, 6: CCD video camera (Philips PCVC740K ToUcam Pro), 7: Pressure transducer (Harvard Apparatus), 8: T adapter with a pressure dome, 9: Clamp, 10: Computer (Acer Aspire 1350 LMi)

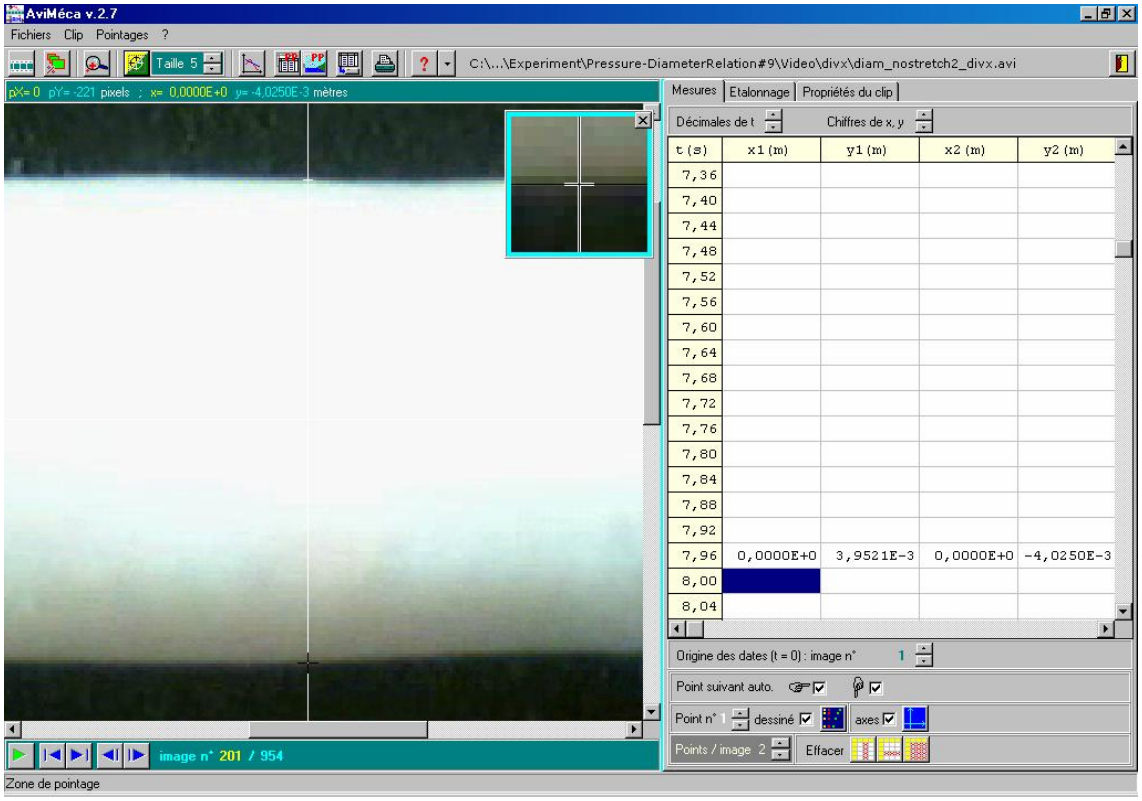

Figure 2.12: AviMéca 2.7 snapshot

Volume

The experimental setup used to measure the diameter of the graft by measuring the change of volume in the vessel chamber is schematically presented in Fig. 2.13.. The pressure application system, rate, and monitoring remains the same as before; however the diameter measurement changes. The vessel chamber is closed hermetically and a 1 mL pipette is inserted into an aperture on the lid. The vessel chamber is filled with water until the liquid starts to fill the pipette. Then, the increase of the diameter of the graft drives the liquid into the pipette. This experiment is possible because water is incompressible. As a consequence, any air bubbles trapped in the vessel chamber must be removed by using the clamp inserted into the lid. The average outer diameter of the graft is calculated by measuring the change of volume in the pipette assuming the graft is a perfect cylinder

$$d_o = \sqrt{\frac{4\left(\Delta V + V_0\right)}{\pi L}}, \tag{2.33}$$

where ΔV is the change of volume in the pipette, $V_0 = \frac{\pi D_o^2}{4} L$, and L is the length of the graft. The digital display of the pressure is behind the pipette. The pressure display and the volume in the pipette are filmed at the same time (Figure 2.14: 10) by a CCD video camera (Philips PCVC740K ToUcam Pro) and recorded on a computer (Acer Aspire 1350 LMi). The volume in the pipette is measured using a video measurement software (AviMéca 2.7.30).

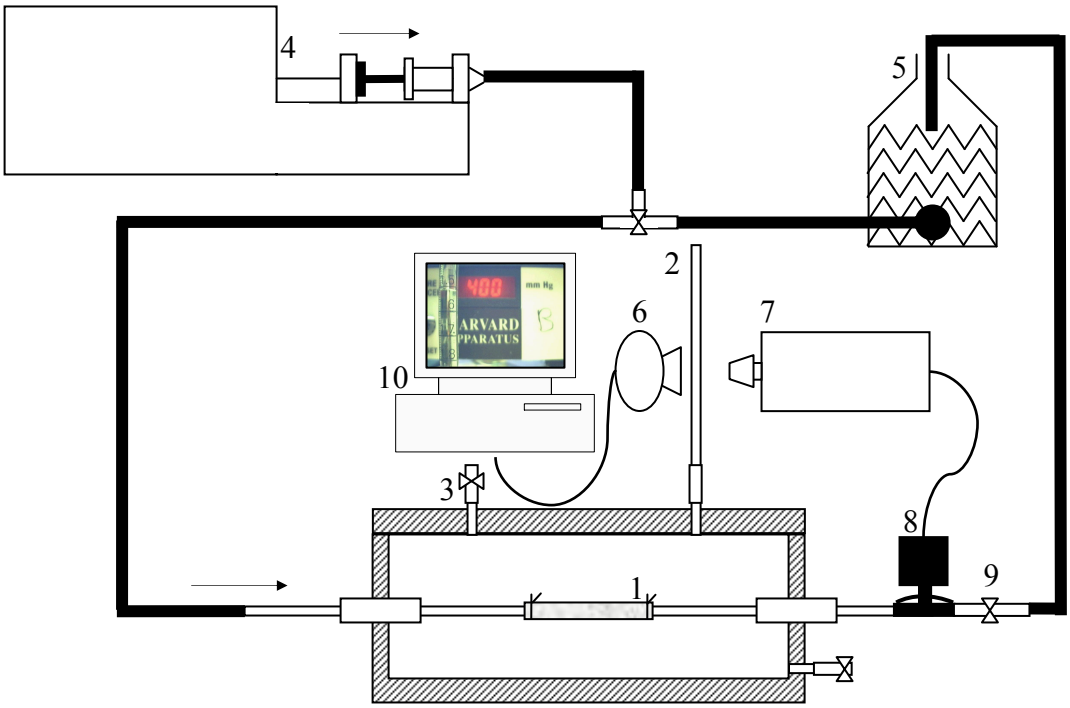

Figure 2.13: Change of volume measurement experimental setup.
1: PVA hydrogel graft sample, 2: 1mL pipette , 3: Clamp to remove air bubble from the vessel chamber, 4: Infusion/Withdrawal Syringe Pump (Harvard Apparatus), 5: Reservoir, 6: CCD video camera (Philips PCVC740K ToUcam Pro), 7: Pressure transducer (Harvard Apparatus), 8: T adapter with a pressure dome, 9: Clamp, 10: Computer (Acer Aspire 1350 LMi)

2.6.5 SEF parameters

The identification of the synthetic hydrogel SEF consists of determining two material constants a and c [13, 45]. According to Eq. (2.30) the natural logarithm of the derivative of the SEF is a linear function of the first invariant:

$$\ln\left(\frac{\partial W}{\partial I_1}\right) = AI_1 + B\,, \tag{2.34}$$

with $A = a$, $B = \ln c - 3a$.

A linear regression of $\ln\left(\frac{\partial W}{\partial I_1}\right)$ versus I_1 determines the SEF parameters, also called material constants a and c

$$a = A\,,\ c = \exp\left(3A + B\right), \tag{2.35}$$

The set of recorded data $\{P_i, d_{oi}\}$ is transformed into a set of experimental stress-stretch data $\{\sigma_i, \lambda_{\theta i}\}$ that are converted into $\left\{\ln\left(\frac{\partial W}{\partial I_1}\right)_i, I_{1i}\right\}$. A linear regression of the set of points $\left\{\ln\left(\frac{\partial W}{\partial I_1}\right)_i, I_{1i}\right\}$ gives the constant $\{A, B\}$, and the material constants $\{a, c\}$ are deduced from Eq. (2.35). The Fig. 2.14 illustrates the process to find the material constant of the synthetic hydrogel and indicates the relation between equations.

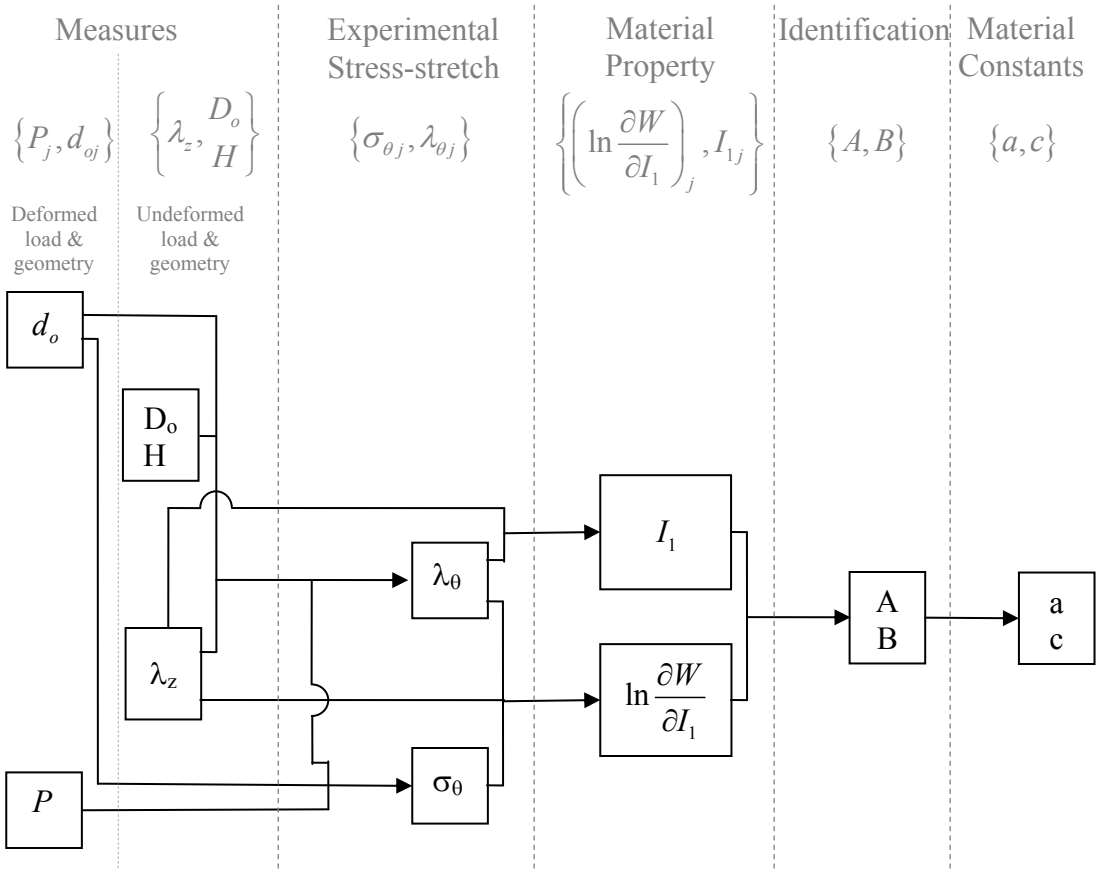

Figure 2.14: Sketch of process and relation to determine synthetic hydrogel material constant

2.6.6 Model validation

The mathematical model is validated by predicting the inflation of a tube longitudinally stretched. The predicted mechanical response is compared to the experimental response.

Two marks are made on the longitudinal axis with ink. The axial stretch ratio is calculated by measuring the distance between those two points before and after the stretching process, as illustrated in Fig. 2.15. The measurement uses a video measurement as described before.

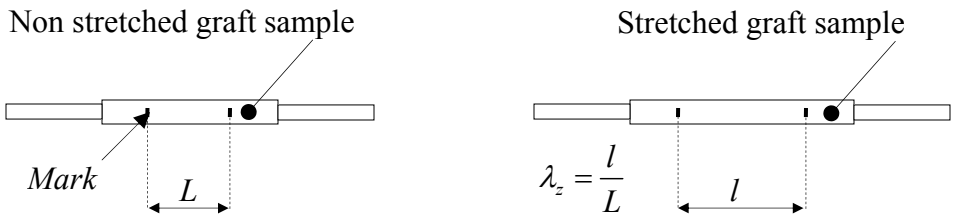

Figure 2.15: Measurement of the axial stretch ratio

2.7 Sensitivity analysis

The sensitivity analysis determines the influence of the host artery parameters ($r_{iam}, E_{pam}, F_{zam}$) on the graft design outcomes (R_i, H, λ_z). If a small change in a parameter results in relatively large changes in the outcomes, the outcomes are said to be sensitive to that parameter (IIASA).

An unidirectional analysis is performed by screening the parameters one by one. This approach does not take into account combined influence of parameters due to the non linearity of the problem (see Eqs (2.10) and (2.20)). However, we are able to determine the less important parameter and keep it a fixed value in order to perform a two directional screening.

This analysis is made for the CCHA and the corresponding IOG. The reference parameters (subscript 0) are ($r_{iam0}, E_{pam0}, F_{zam0}$) of the CCHA from [54] at a mean pressure of 100 mmHg. The parameter is screened from -30% to +30% of its reference values, i.e.

$$0.7 < \frac{P}{P_0} < 1.3,$$

where P is the screened parameter. The other non screened parameters are kept at their reference values. The outcomes are calculated using the Maple code given in Appendix B and normalized in order to compare their respective sensitivity.

2.8 Burst pressure

A burst pressure test is performed on the graft prototype from which the ultimate circumferential stress is determined. The burst pressure test setup is the same as the "cross section" pressure-diameter setup. The inflation of the graft prototype is made at rate of 1 mmHg/s until it bursts. The circumferential ultimate stress, also called burst stress, is estimated solving the problem of finite inflation and extension of a cylindrical tube using the Maple code in Appendix A. the burst pressure is then predicted for the other untested tubes by using equation 2.13 and assume the ultimate stress is the same between the tubes.

2.9 Selection algorithm

A selection algorithm is elaborated to select the graft that best fits one individual host artery from a set of manufactured grafts.

Non invasive measurement of artery in vivo

The aim of a non invasive measurement technique is to measure the patient's host artery diameter and pressure responses in order to identify the host artery parameters and select the manufactured graft that best matches the host artery. The sensitivity analysis in Section 2.4.2 shows that the force can be determined with a very low accuracy. Thus, the axial force F_{zam} is not measured for each patient, but its reference value F_{zam0} (from literature) is taken instead. Then the parameters of the host artery reduce to $d_{iam}^{Patient}$,

$E_{pam}^{Patient}$, F_{zam0}, where the superscript "Patient" indicates that those values are specific to a patient.

A high-resolution ultrasonic echo-tracking device (NIUS 02®, SMH, Bienne, Switzerland) can be used to measure the internal diameter [55]. This device was described and validated for the measurement of radial parameters in humans [4]. The diameter is measured measuring the time between two peaks of the RF ultrasound signal that is acquired with a 10-MHz probe as illustrated in Fig. 2.16.

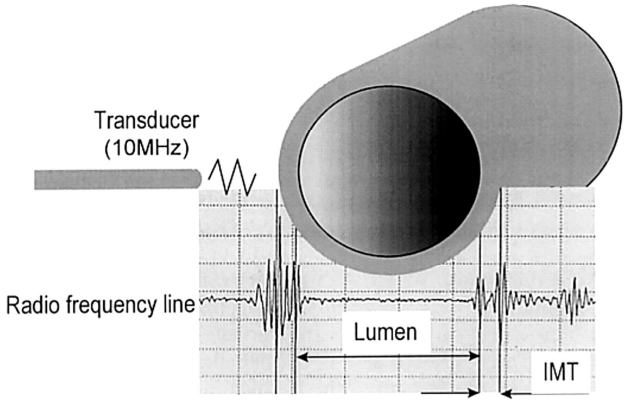

Figure 2.16: Schematic illustration of the arterial diameter determination by an A-mode echo-tracking system (NIUS 2). The cursors automatically focus on the echogenic interfaces delineating the wall lumen [57]
, IMT: intima-media thickness.

The system is coupled to a digital photo-plethysmograph finger cuff (FMS, Finapres Measurement Systems, Arnhem, Netherlands) for simultaneous blood pressure measurements. Because the pressure and diameter are measured at different sites, the two signals are delayed. They are synchronized using a model based on wave speed [55]. The inner diameter resolution is 160 µm for absolute values (2.5 µm during systolic-diastolic

changes) and the pressure resolution is about 2 mmHg. A preprocessing signal analysis software can calculate the mean pressure by integration and returns the diameter at the mean pressure as illustrated in Fig. 2.17. It returns also the systolic and diastolic values of pressure and inner diameter. These parameters are the input of the "program for selection" that selects the best manufactured graft for the patient. The overall process from measurement to selection is illustrated in Fig. 2.18. The program is detailed in Section 3.2.

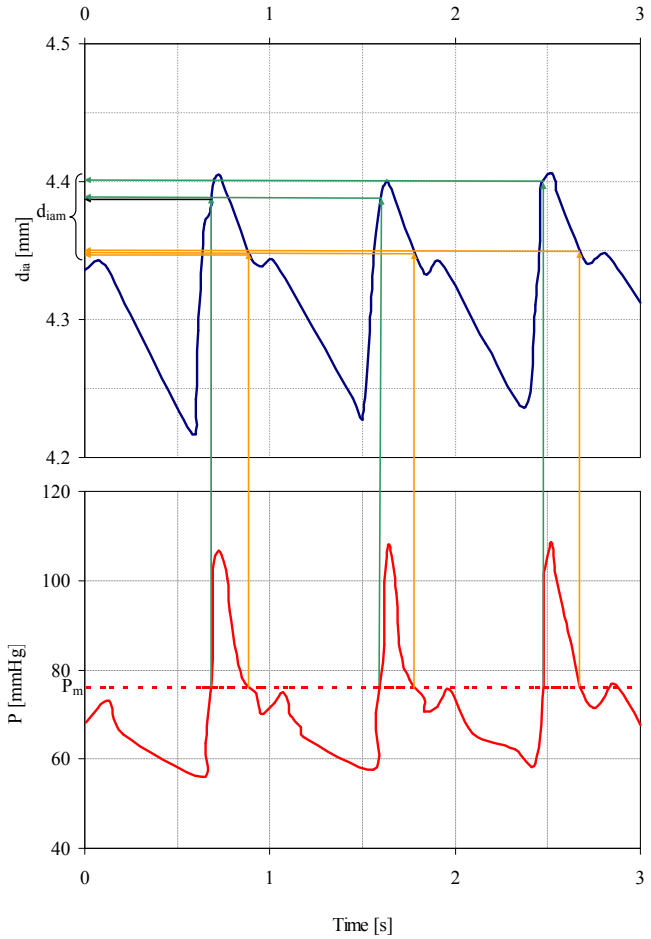

Figure 2.17: Continuous and simultaneous pressure (bottom) diameter (top) record and inner diameter at mean pressure identification

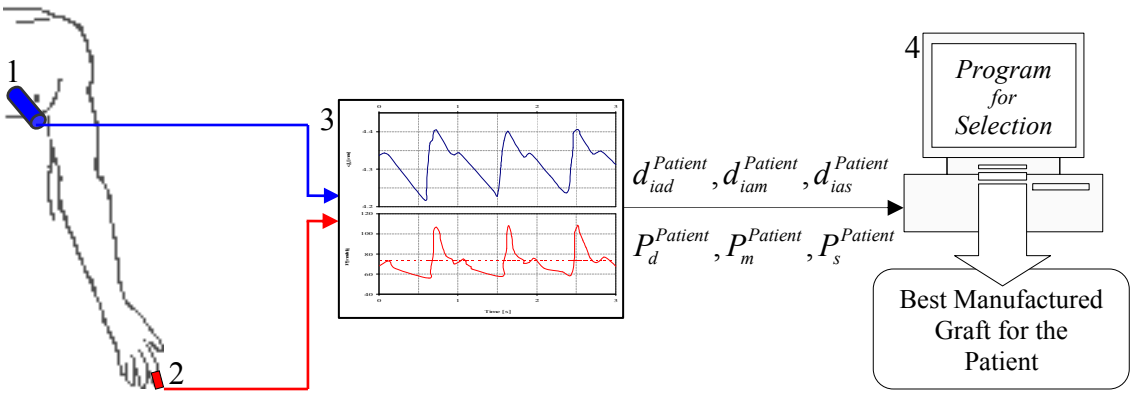

Figure 2.18: Schematic representation of the setup to measure simultaneously the pressure and the diameter of one individual host artery and select the best manufactured graft, 1: Ultrasonic transducer (record the inner diameter of the Host Artery), 2: Digital photo-plethysmograph finger cuff (record the blood pressure), 3. Preprocessing software (captures and analyses the signals : return the diastolic, mean and systolic values), 4: The "Program for selection" returns the best graft for the patient

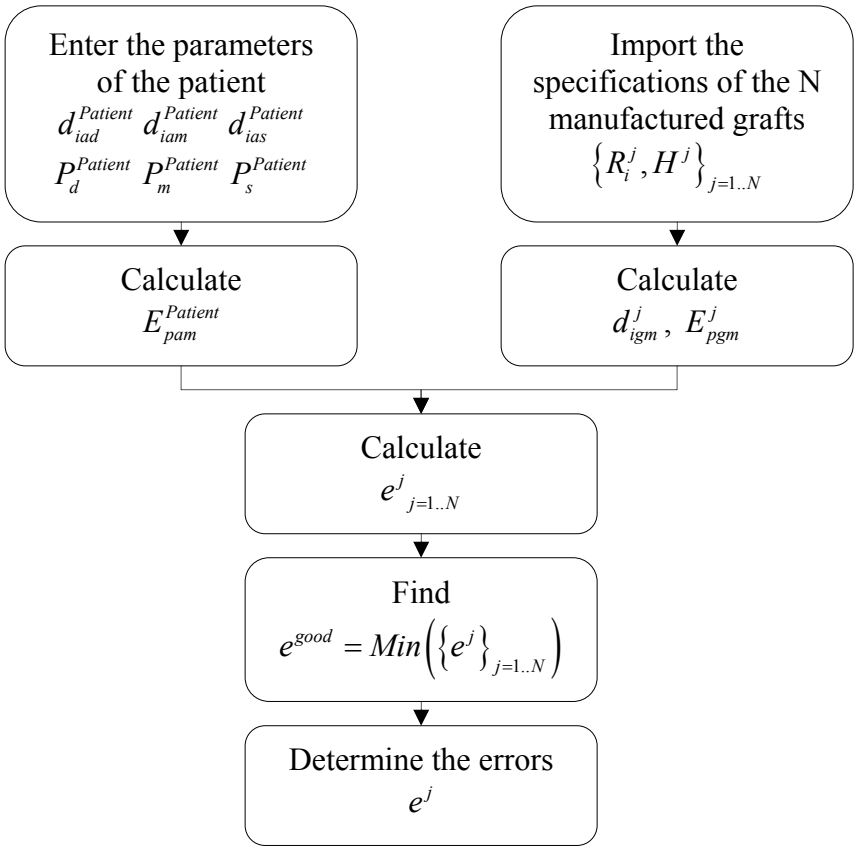

Figure 2.19: Logic block diagram to determine the manufactured graft that best fit the patient characteristics

Procedure of graft selection

The best graft for the patient is the graft whose mechanical responses are closest to the mechanical responses of the host artery of the patient. The mechanical equivalence has been defined before by the "one point criterion". Then the manufactured graft that best fit the host artery is the one that minimizes the errors of the inner diameter and Peterson modulus between the graft and the host artery at the mean pressure. The axial stretch ratio prior to implantation is set to one because this simplifies the surgical procedure of implantation. The error is defined as the weighted Euclidian distance between the graft and the host artery in the diameter and Peterson modulus plan at the mean pressure of the Patient

$$e^j = w\left(\frac{d_{am}^{Patient} - d_{gm}^{j}}{d_{gm}^{j}}\right)^2 + (1-w)\left(\frac{E_{pam}^{Patient} - E_{pgm}^{j}}{E_{pgm}^{j}}\right)^2 \tag{2.36}$$

where $0 < w < 1$ is the weighting factor and the subscript "j" indicates that the value refers to the manufactured graft number j. According to the sensitivity analysis, the diameter has more importance than the Peterson modulus. That's why w is taken greater (w=0.6) than $\frac{1}{2}$. The Peterson modulus is calculated from measured parameters from the patient as follows

$$E_{pam}^{Patient} = \frac{\left(P_d^{Patient} - P_s^{Patient}\right)}{d_{ias}^{Patient} - d_{iad}^{Patient}} \cdot d_{iam}^{Patient} \tag{2.37}$$

The program of selection entitled "Selection of the best MG for the patient" (Appendix C) follows the logic block diagram given in Fig. 2.19.

CHAPTER 3

RESULTS

3.1 Choice of material

PVA hydrogel is chosen as an example material to create a mechanics-matching graft. This material could be manufactured under a variety of ways within the laboratory at G.I.T.

Current synthetic graft material

Current approved clinical synthetic grafts are made of Dacron (PTE) and Gore-Tex (ePTFE), which are very stiff materials compared to native arteries. The thicknesses of the current graft in order to be compliant are given in Table 3.1.

Table 3.1: Thickness of current graft to be compliant

	h_g [mm]
Dacron (PET)	$1.18\ 10^{-04}$
Gore-Tex (ePTFE)	$5.89\ 10^{-04}$

h_g: thickness of the current graft

Grafts made of Dacron or ePTFE would have dimensions which are difficult to manufacture. Besides such thin wall grafts would have a very low burst pressure resistance. Thus it is necessary to seek another material.

PVA hydrogel tubes

The thickness (Table 3.2.) can be manufactured and may confer a great burst pressure resistance. This demonstrates that when correctly processed and design, PVA hydrogel can be used for fabricating compliant arterial grafts.

Table 3.2: Range of thickness of a possible compliant tube made of PVA hydrogel and corresponding stiffness.

	E_g [MPa]	h_g [mm]
PVA hydrogel	0.61	0.65
	1.01	0.23

Eg: Young's modulus of PVA hydrogel, hg: thickness of tube mode of PVA hydrogel

Moreover PVA hydrogel combines properties such as biocompatibility, hydrophilicity, permeability [25] and ease of manufacture [8]. As a consequence PVA hydrogel is the material chosen to design a mechanics matching graft.

3.2 Pressure-diameter curves of the tube for identification

A tube made of PVA hydrogel is fabricated in order to identify the SEF of the material (in term of material constants a and c) with pressure diameter measurements.

3.2.1 Initial geometry

The outer diameter is measured when the graft mounted in the experimental setup. The inner diameter is measured using the least square method described Chapter 2 and illustrated in Fig. 3.1. The thickness is calculated from these two measurements.

$$D_o = 7.885mm\left(\pm 0.032, n = 3\right)$$

$$D_i = 4.885mm\left(\pm 0.011, n = 3\right),\ e = 0.0066mm^2$$

$$H = 1.50mm$$

The tube is close (R/H=2.13) to be thin-wall (R/H=5) at its unloaded configuration. A pressurized tube tends to the thin-wall assumption as the thickness decreases and radius increases. Tubes verifying the thin-wall assumption have mechanical responses within 5% of their thin-wall model mechanical responses predictions.

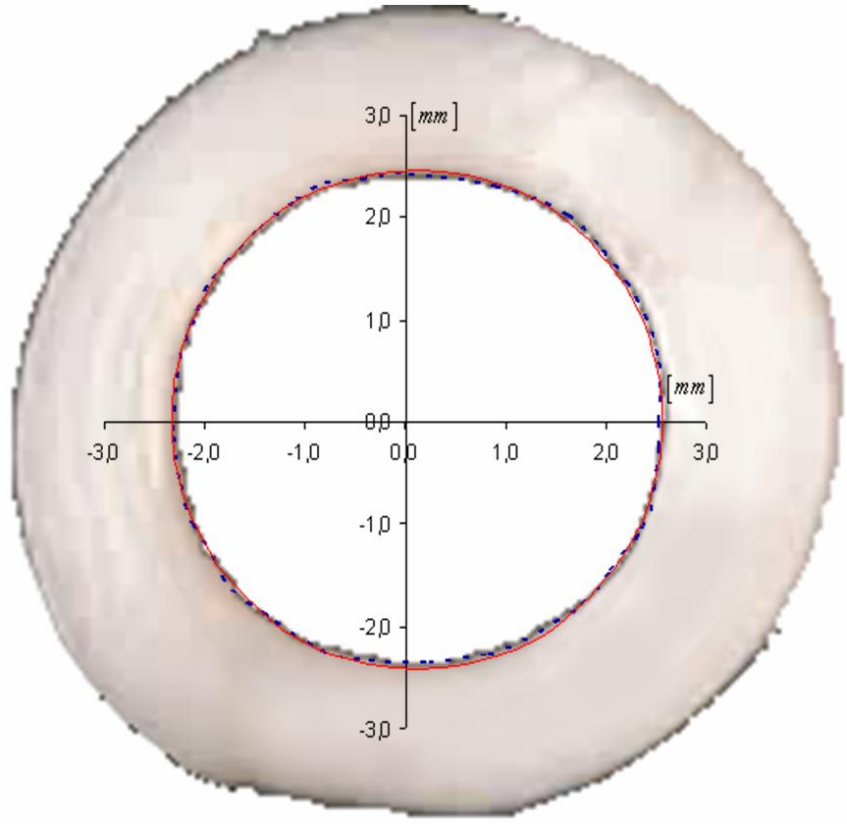

Figure 3.1: Measured (dashed blue line) and average (solid red line) inner diameter of the tube

3.2.2 Cross-section

Table 3.3: Pressure-diameter relation ("cross-section" measurement)

P [mmHg]	d_o [mm]	d_o/D_o [-]
0	7.885 (±0.032)	1.000
20	7.918 (±0.006)	1.004
40	7.957 (±0.007)	1.009
60	7.976 (±0.021)	1.012
80	8.024 (±0.008)	1.018
100	8.066 (±0.044)	1.023
120	8.115 (±0.023)	1.029
140	8.139 (±0.007)	1.032
160	8.212 (±0.023)	1.041
180	8.248 (±0.007)	1.046
200	8.303 (±0.030)	1.053
220	8.369 (±0.018)	1.061
240	8.430 (±0.036)	1.069
260	8.496 (±0.008)	1.078
280	8.539 (±0.021)	1.083
300	8.587 (±0.023)	1.089
320	8.654 (±0.014)	1.098
340	8.708 (±0.015)	1.104
360	8.751 (±0.023)	1.110
380	8.823 (±0.023)	1.119
400	8.884 (±0.031)	1.127

P: Pressure; D_o: Non deformed outer diameter; d_o: Outer diameter expressed as Mean ±S.E., n=3

3.2.3 Volume

Table 3.4: Pressure-diameter relation ("volume" measurement)

P [mmHg]	d_o [mm]	d_o/D_o [-]
0	7.885 (±0.032)	1.000
20	7.913 (±0.006)	1.004
40	7.947 (±0.010)	1.008
60	7.979 (±0.013)	1.012
80	8.013 (±0.013)	1.016
100	8.048 (±0.011)	1.021
120	8.093 (±0.009)	1.026
140	8.134 (±0.010)	1.032
160	8.177 (±0.008)	1.037
180	8.224 (±0.012)	1.043
200	8.269 (±0.012)	1.049
220	8.316 (±0.010)	1.055
240	8.379 (±0.008)	1.063
260	8.426 (±0.009)	1.069
280	8.479 (±0.008)	1.075
300	8.531 (±0.008)	1.082
320	8.578 (±0.010)	1.088
340	8.630 (±0.014)	1.094
360	8.678 (±0.009)	1.101
380	8.724 (±0.011)	1.106
400	8.775 (±0.008)	1.113

P: Pressure; D_o: Non deformed outer diameter; d_o: Outer diameter expressed as Mean ±S.E., n=3

3.2.4 Comparison

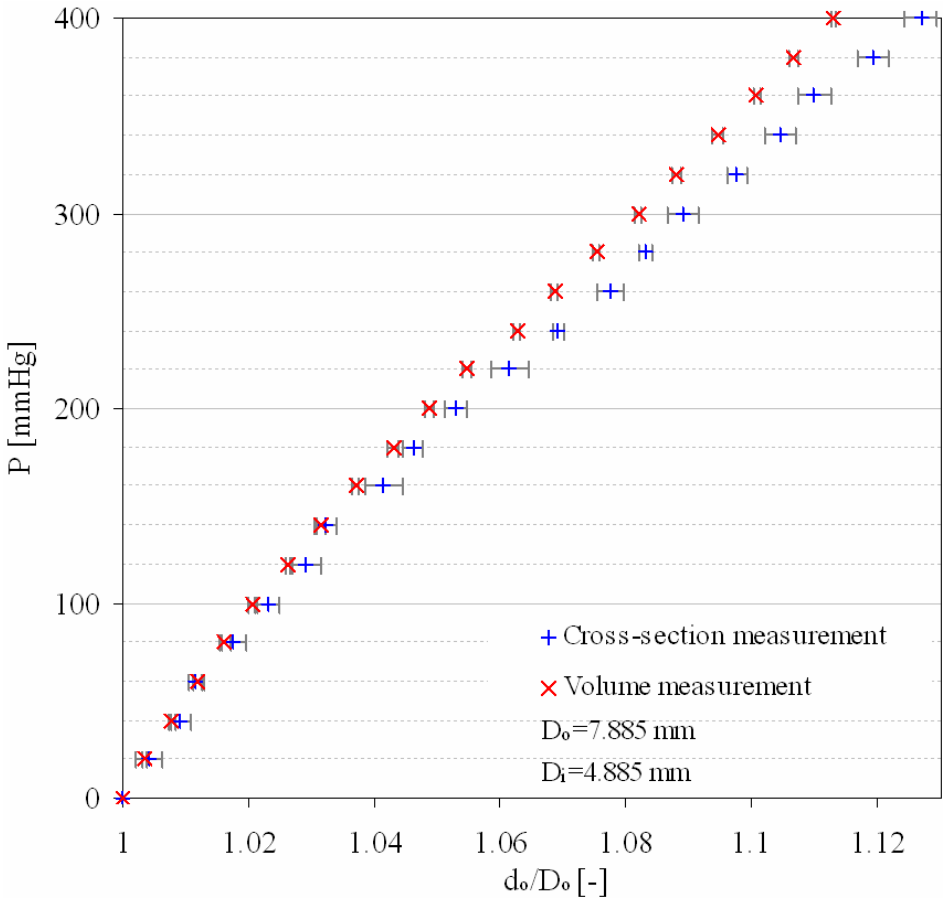

Figure 3.2: Pressure-diameter relationship of the graft at an axial stretch ratio of one. (Bars: S.E., n=3)

3.2.5 Differences

The difference between the two experiments is calculated as follows

$$diff = \frac{d_{ov} - d_{ol}}{d_{ol}},$$

where the indices l indicates that the value is given by the local diameter measurement experiment and v indicates that the value is given by the change of volume experiment.

Table 3.5: Differences in the diameter measurement between the two experiment setups

P [mmHg]	Differences [%]
0	0.00
20	-0.06
40	-0.13
60	0.05
80	-0.14
100	-0.23
120	-0.27
140	-0.06
160	-0.42
180	-0.29
200	-0.40
220	-0.63
240	-0.60
260	-0.83
280	-0.70
300	-0.65
320	-0.88
340	-0.90
360	-0.83
380	-1.13
400	-1.23

P: Pressure

The differences between the "cross-section" and "volume" measurements are small (around 1%). The outer diameters obtained from the "volume" measurement are smaller than those obtained from the "cross-section" measurement, because the tube does not deform as a perfect cylinder (edge effect shown in Fig. 3.3.). Both measurements should tend to the same values, when the tube is long enough. But this is not the case in our setup. In the following only data obtained from the "cross-section" measurement are used, as they reflect more the deformation of the cylindrical tube used in the model.

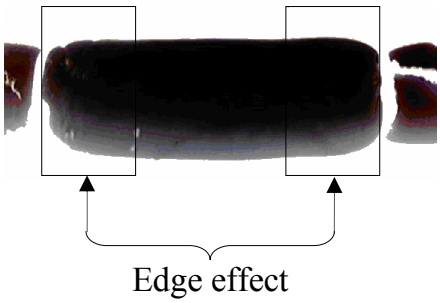

Figure 3.3: Description of the edge effect @P=400 mmHg (negative image)

3.3 SEF parameters

The SEF parameters (material constant a and c) determine the material properties. Data from Table 3.3 are used to calculate the mechanical responses given in Table 3.6.

Table 3.6: Mechanical responses of the tube for SEF identification (λ_z=1.0)

P [mmHg]	λ_θ [-]	E_θ [-]	σ_θ [kPa]	I_1 [-]	Ln(dW/dI_1) [-]
0	1.000	0.000	0.00	3.0000	-
20	1.007	0.007	4.42	3.0002	4.402
40	1.015	0.015	9.02	3.0009	4.340
60	1.018	0.019	13.66	3.0013	4.535
80	1.028	0.029	18.67	3.0031	4.427
100	1.037	0.037	23.84	3.0052	4.412
120	1.046	0.048	29.29	3.0083	4.388
140	1.051	0.053	34.57	3.0100	4.457
160	1.066	0.068	40.90	3.0162	4.384
180	1.073	0.076	46.79	3.0198	4.418
200	1.084	0.087	53.30	3.0258	4.415
220	1.097	0.101	60.40	3.0341	4.400
240	1.108	0.114	67.66	3.0425	4.402
260	1.121	0.129	75.41	3.0526	4.403
280	1.129	0.138	82.67	3.0595	4.432
300	1.139	0.148	90.37	3.0678	4.455
320	1.151	0.163	99.04	3.0800	4.462
340	1.162	0.175	107.53	3.0905	4.481
360	1.170	0.184	115.77	3.0991	4.509
380	1.183	0.200	125.68	3.1145	4.517
400	1.195	0.214	135.37	3.1280	4.534

P: Pressure; λ_θ: Circumferential stretch ratio; E_θ: Circumferential Green's strain; σ_θ: Circumferential Cauchy stress; I_1: First invariant; W: Strain Energy Density Function.

The set of points $\left\{ \ln\left(\frac{\partial W}{\partial I_1}\right)_i, I_{1i} \right\}$ are the plotted as illustrated in Fig. 3.4.

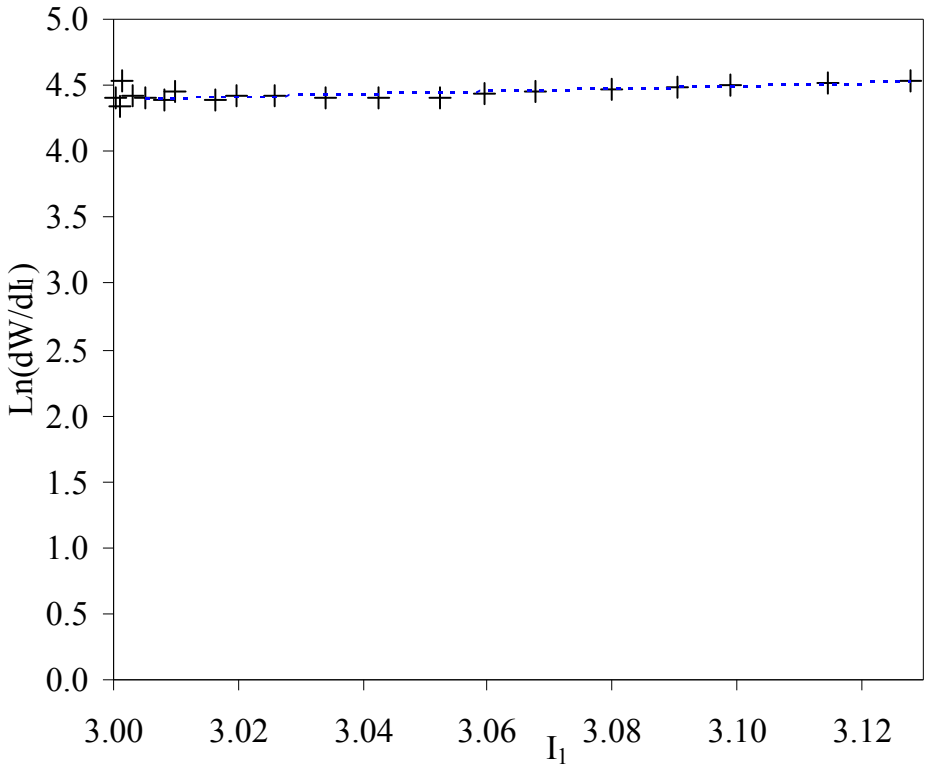

Figure 3.4: Experimental $\{\text{Ln}(dW/dI_1)_i, I_{1i}\}$ set of points and its linear regression

The set of points $\left\{\ln\left(\frac{\partial W}{\partial I_1}\right)_i, I_{1i}\right\}$ are around a straight line. A linear regression of these points (from 40 mmHg to 400 mmHg) gives the constant $A = 0.8503$ and $B = 1.8514$, and the material constants are

$$a = 0.85$$

$$c = 81.625\ kPa$$

3.4 Model validation

The model is validated by predicting the mechanical response of the tube when it is initially stretched. The axial stretch ratio is set to $\lambda_z = 1.038$. Table 3.7. shows the experimental and theoretical mechanical responses.

Table 3.7: Experimental and theoretical mechanical responses of the tube for SEF identification with an axial stretch ratio of 1.038

	Experimental mechanical reponses			Theoretical mechanical responses		
P	d_o	E_θ	σ_θ	d_o	E_θ	σ_θ
[mmHg]	[mm]	[-]	[kPa]	[mm]	[-]	[kPa]
0	7.699 (±0.128)	-0.026	0.00	7.739	-0.018	0.00
20	7.718 (±0.152)	-0.023	4.29	7.773	-0.012	4.42
40	7.730 (±0.138)	-0.020	8.64	7.809	-0.004	9.00
60	7.772 (±0.118)	-0.012	13.26	7.846	0.003	13.79
80	7.827 (±0.133)	-0.001	18.20	7.885	0.011	18.75
100	7.864 (±0.133)	0.007	23.18	7.926	0.019	23.93
120	7.900 (±0.123)	0.014	28.34	7.969	0.028	29.34
140	7.967 (±0.122)	0.028	34.20	8.014	0.037	34.99
160	8.015 (±0.093)	0.038	40.02	8.061	0.047	40.91
180	8.076 (±0.131)	0.050	46.36	8.111	0.058	47.12
200	8.149 (±0.102)	0.066	53.29	8.163	0.068	53.63
220	8.216 (±0.104)	0.080	60.43	8.217	0.080	60.46
240	8.253 (±0.095)	0.087	67.01	8.274	0.092	67.65
260	8.344 (±0.088)	0.106	75.55	8.333	0.104	75.20
280	8.423 (±0.071)	0.123	84.13	8.394	0.117	83.14
300	8.502 (±0.058)	0.140	93.13	8.458	0.131	91.48
320	8.551 (±0.085)	0.151	101.33	8.524	0.145	100.26
340	8.618 (±0.064)	0.165	110.57	8.592	0.160	109.46
360	8.685 (±0.042)	0.180	120.16	8.661	0.174	119.11
380	8.739 (±0.075)	0.192	129.54	8.732	0.190	129.21
400	8.806 (±0.048)	0.207	139.83	8.805	0.206	139.77

P: Pressure; d_o: Outer diameter expressed as Mean ±S.E., n=3; E_θ: Circumferential Green's strain; σ_θ: Circumferential Cauchy stress.

The comparison of the experimental and theoretical responses is made on the stress-strain response illustrated in Fig. 3.5..

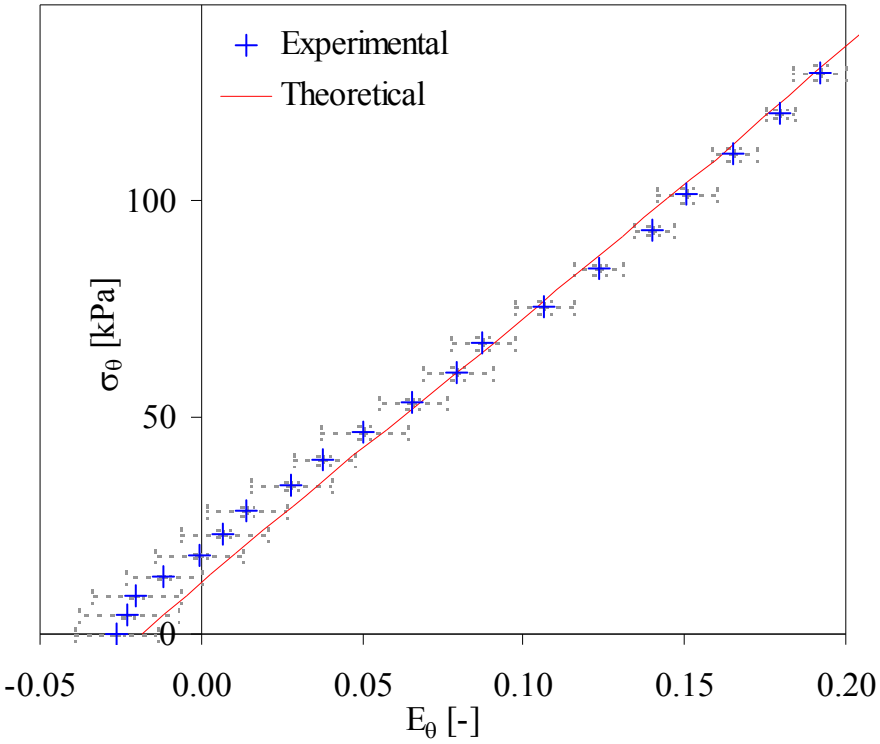

Figure 3.5: Experimental and theoretical Stress-strain relationship at an axial stretch ratio of 1.038. (bars: S.E.)

The correlation between the experimental and theoretical set of points is calculated using the Pearson Product Moment correlation, as follows

$$r = 0.999936$$

This good correlation between theoretical predictions and experimental data validates the mathematical model.

3.5 Design of mechanics-matching grafts

In the following, the design optimization is applied to a canine and human model.

Canine carotid host artery (CCHA)

The ideal optimized graft (IOG) dimensions are calculated for a mean pressure of 100 mmHg. The inner diameter, Peterson modulus and axial force of the host artery are respectively equal to $d_{iam} = 4.115mm$, $E_{pam} = 67.0kPa$ and $F_{zam} = 51.8N$ (see Table 2.12). Using the Maple program given in Appendix B, the IOG initial dimensions and axial stretch ratio are calculated

$$R_i = 1.867\text{mm},\ H = 0.360\text{mm},\ \lambda_z = 1.160$$

The mechanical responses of the IOG given in Table 3.8 are predicted using the mathematical model (Maple's code in Appendix A). At a mean pressure of 100 mmHg, the mid wall radius is $r = 2.202$ mm, the thickness is $h = 0.289$ and the ratio $\frac{r}{h} = 7.620 > 5$. Thus, in the range of interest, i.e. around the mean pressure, the membrane model is verified. The fit between the pressure diameter relationships of the CCHA and the IOG is shown in Fig. 3.6.

Table 3.8: Mechanical responses of the IOG for a CCHA calculated from the membrane model

P [mmHg]	d_{ig} [mm]	E_{pg} [kPa]	F_{zg} [g]
0	3.467	96.6	33.4
20	3.569	88.1	36.3
40	3.684	80.5	39.5
60	3.813	74.3	43.1
80	3.957	69.7	47.2
100	4.115	67.0	51.8
120	4.283	66.4	57.0
140	4.457	67.9	62.7
160	4.632	71.5	69.0
180	4.802	76.9	75.7
200	4.964	84.0	82.7
220	5.117	92.3	90.0
240	5.259	101.8	97.6

P: pressure; d_{ig}: inner diameter; E_{pg}: Peterson modulus; F_{zg}: axial force

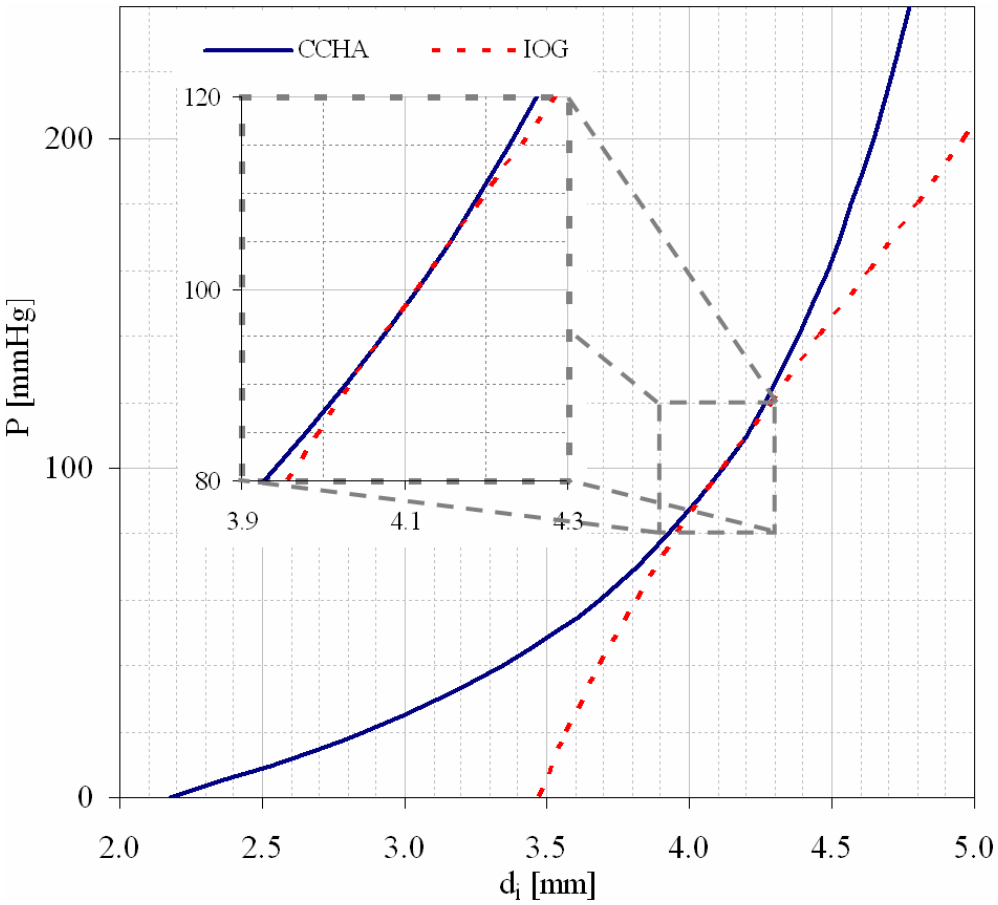

Figure 3.6: Pressure-diameter (P-D) relationship of the CCHA (solid line) and predicted P-D relationship of the IOG (dashed line)

Human coronary host artery (HCHA)

The fabrication parameters for the HCHA are given in Table 3.9.

Table 3.9: Design outcomes for a human coronary host artery

F_z [g]	λ_z [-]	R_i [mm]	H [mm]
5	0.996	2.093	6.325
50	1.000	2.097	6.447

F_z: supposed axial force of the host artery, λ_z: axial stretch ratio of the ideal graft, R_i: inner radius of the ideal graft, H: thickness of the ideal graft.

The thickness of the human IOG is greater than that of canine IOG because the human coronary arteries are stiffer than canine carotid artery.

3.6 Sensitivity analysis

The sensitivity analysis shows that the host artery parameters do not need to be precise and that the longitudinal stretch ratio of the graft is not so important.

Screening of one parameter

Only one parameter is screened while the others are kept constant. The results are given in Figure 3.7. The axial force of the artery has almost no effects on the design outcome and can then be determined with a very low accuracy.

Screening of two parameters

The axial force parameter is kept constant while the diameter and the Peterson modulus of the host artery are simultaneously screened. The results are given in Figure 3.8.

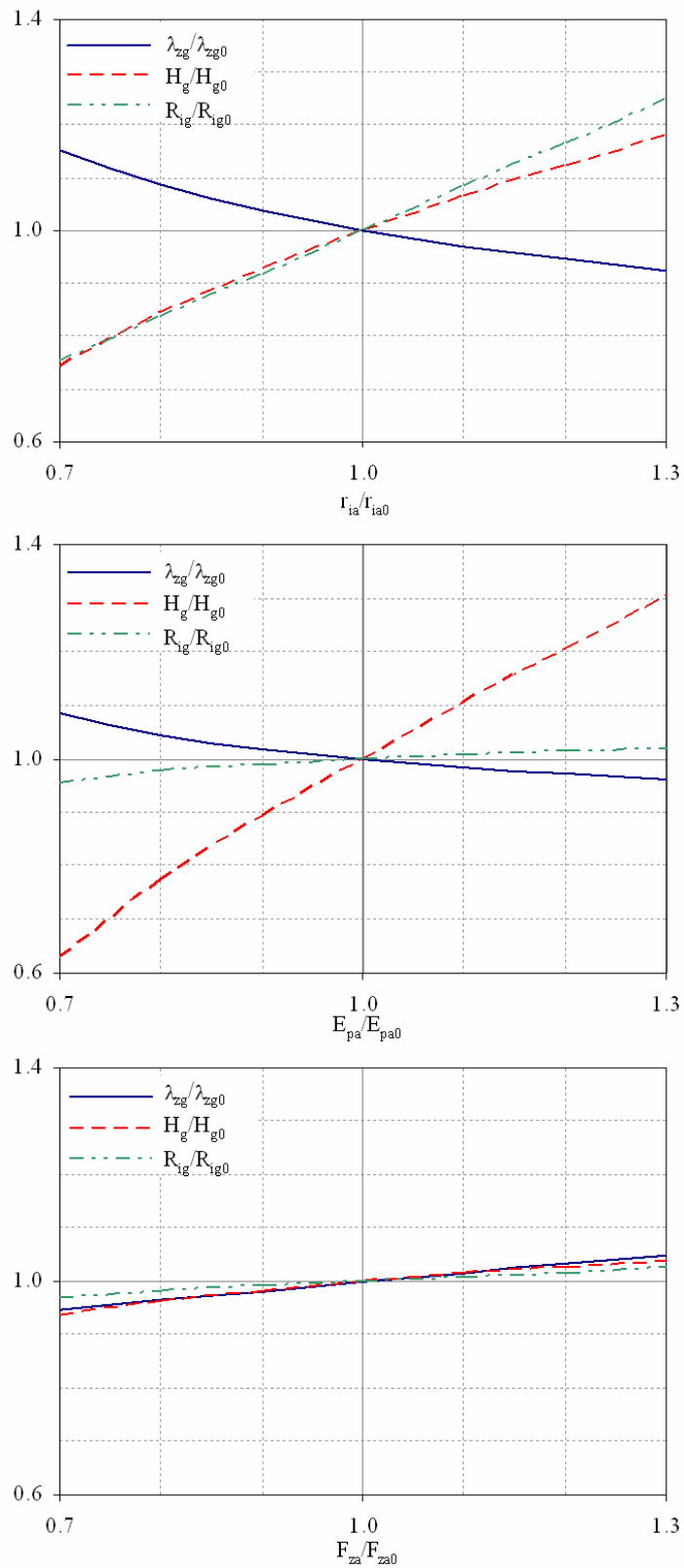

Figure 3.7: One parameter screening, X-coordinate: the screened parameter, Y-coordinate: the outcomes variation, r_{iam0}=4.115/2 mm, E_{pam0}=67.0 kPa, F_{zam0}=51.8 N, R_{i0}=1.867 mm, H_0=0.360 mm, λ_{z0}=1.160

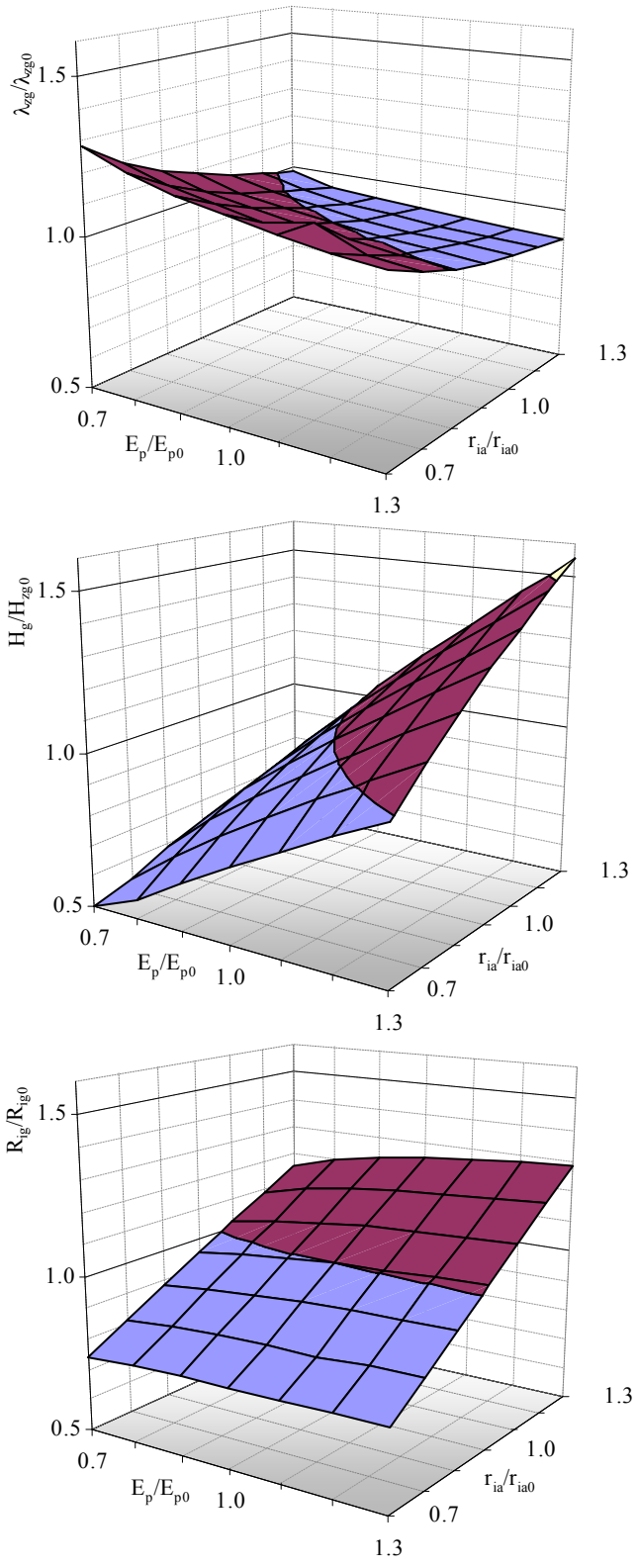

Figure 3.8: Screening of two parameters (X-Y plan: the two parameters screened, Z-coordinate: the outcome variation)

Sensitivity of λ_{zg}

The non linearity of the problem is seen in the sensitivity analysis of the axial stretch ratio. The axial stretch ratio appears to be sensitive only when both the functional stiffness and radius of the host artery decrease. Then, λ_{zg} can be determined with a low accuracy when the Peterson modulus and radius of the host artery are greater than their reference values.

Sensitivity of H_g

The thickness is highly sensitive to the functional stiffness and radius of the host artery. For a variation of $\pm 30\%$ of these parameters, the thickness varies between -50% and $+60\%$ of its reference value. Thus, the Peterson modulus and diameter of the host artery must be determined with an extremely high accuracy. For a given radius, an increase of the functional stiffness is compensated by an increase in the thickness of the graft. This result is in concordance with the Eq. (2.23). The thickness of the graft appears to be an alternative to control the functional stiffness of the graft for a given diameter.

Sensitivity of R_{ig}

The radius of the graft is mainly sensitive to the radius of the host artery. This confirms that the radius of the graft must be determined with a high accuracy.

Summarizing, the radius of the host artery must be determined with a high accuracy because the radius and the thickness of the graft are very sensitive to this parameter. The functional stiffness of the host artery affects mainly the thickness of the graft. The axial force of the host artery has almost no influence on the design outcomes and can be determined with an extremely low accuracy.

3.7 Possible range of fabrication

Designing and building a specific graft for an individual is not practical. Fabricating a set of grafts with a range of mechanical responses is more realistic. We were able to design a mechanics matching graft for a given canine carotid host artery (expected reference). To evaluate the range of mechanical responses the manufactured grafts should cover, a representative sample of canine carotid mechanical responses is taken from [51].

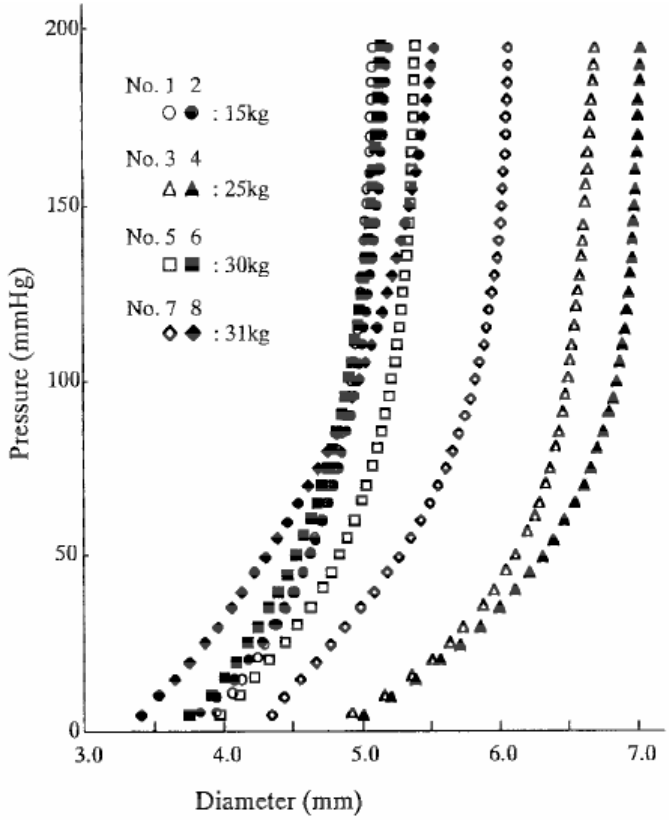

Figure 3.9: P-D relationship of canine common carotid arteries (n = 8) [51], open = right carotid arteries; closed = left carotid arteries.

The mechanical responses (outer diameter and Peterson modulus at mean pressure of 100mmHg) of the representative sample are compared to the expected reference (Table 3.10).

Table 3.10: Mechanical responses of the reference and representative sample canine host artery

	Mechanical responses		Deviation from reference	
	d_o [mm]	E_p [kPa]	$E(d_o)$ [%]	$E(E_p)$ [%]
Reference	4.58	67	0	0
No. 1	4.92	179	8	167
No. 2	4.96	153	8	129
No. 3	6.50	243	42	262
No. 4	6.84	164	49	144
No. 5	5.24	152	15	127
No. 6	4.90	135	7	101
No. 7	5.83	121	27	81
No. 8	4.99	65	9	-3

d_o: outer diameter at 100mmHg, E_p: Peterson modulus, e(x): error of x between representative sample and reference.

The range could cover 100% to 150% of the deformed diameter and 90% to 260% of the functional stiffness of the expected host artery reference. The axial stretch ratio prior to implantation is set to one because this simplifies the surgical procedure of implantation. The Maple program in Appendix B (with $\lambda_z = 1$) is used to evaluate the design range that follows

$$0.25mm < H < 1.35mm$$

$$1.7mm < R_i < 2.9mm$$

3.8 Selection of one prototype

A set of six graft prototypes were manufacture (following the same processing and composition used to fabricate the tube from which the SEF was determined) within the possible range of fabrication. Their dimensions and predicted Peterson modulus are given in Table 3.11.

Table 3.11: Manufactured Graft initial dimensions and predicted compliance

	Prototype Graft #					
	1	2	3	4	5	6
R_i [mm]	1.43	1.74	1.76	1.81	1.82	2.17
H [mm]	0.79	0.92	0.44	0.42	0.72	0.49
E_p [kPa]	200	192	98	91	150	50

R_i: initial inner radius, H: initial thickness, E_p: Predicted Peterson modulus at 100 mmHg

The carotid artery No. 5 is chosen as host artery because it relates an average behavior among all representative carotid samples (Fig. 3.9). The algorithm of selection (Appendix C) returns the graft prototype #5 as the graft that best fit the carotid artery No. 5 at 100 mmHg. The misfit of compliance and diameter is less than 5%, as illustrated in Fig. 3.10.

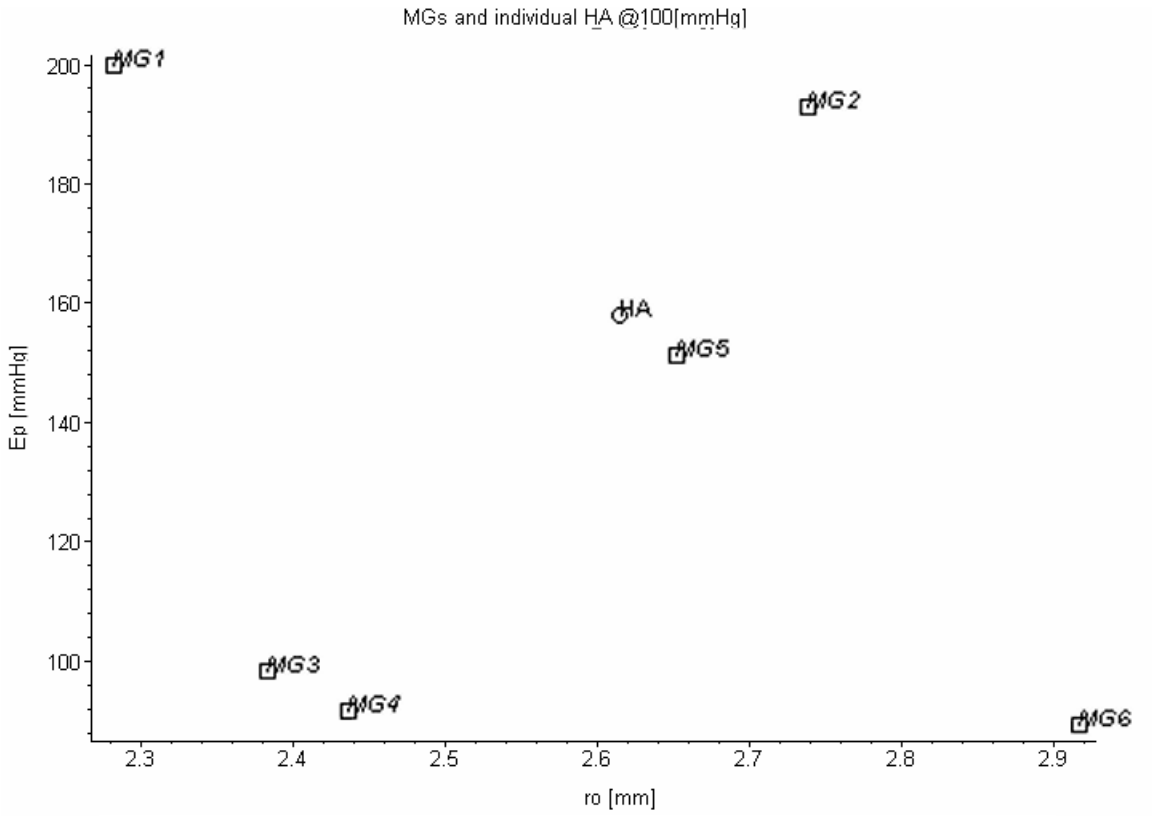

The optimal graft for this patient is the Manufacture Graft # 5, labelled :

[1.82, 150]

[Geometrical,Compliance] mismatch in [%]:

[1.408, -4.360]

Figure 3.10: Algorithm selection (Appendix D) snapshot
MG: Manufactured graft, HA: Host artery

3.9 Picture of the prototype graft #5

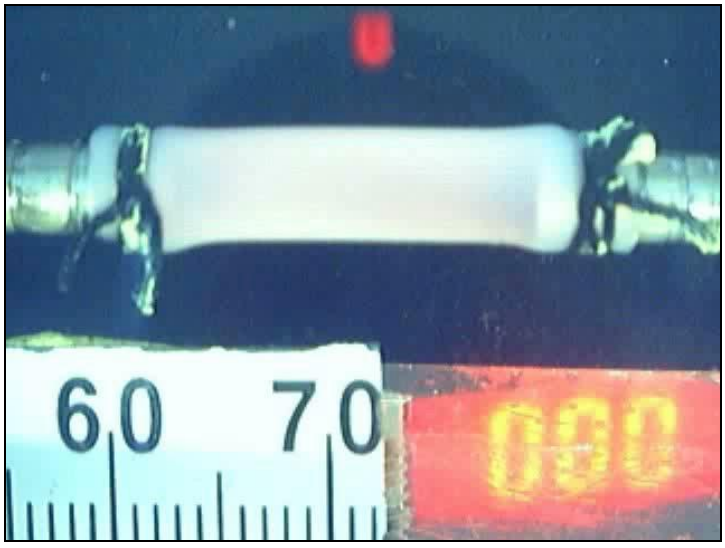

Figure 3.11: Picture of the prototype graft #5 mounted into the experimental setup

3.10 Deviation from prediction

The experimental and predicted responses of the prototype are compared to verify the accuracy of the processing.

The predicted pressure diameter relationship of the graft prototype #5 is calculated solving the problem of finite inflation and extension of a cylindrical tube using the Maple code in Appendix A. The experimental pressure-diameter relationship is determined by the "cross section" experiment. The deviation between the predicted and experimental diameter is less than 2.5% as shown in Table 3.12. the resulting error on the Peterson modulus is about 6% at 100mmHg. Predicted and experimental pressure-diameter relationships are illustrated in Fig. 3.12 with the response of the carotid No. 5

host artery. The predicted and experimental responses of the graft prototype #5 are normalized in the Fig. 3.12.

Table 3.12: Theoretical and experimental mechanical responses of the prototype

	Theoretical		Experimental			Errors	
P	d_i	E_p	d_o	d_i	E_p	$e(d_o)$	$e(E_p)$
[mmHg]	[mm]	[kPa]	[mm]	[mm]	[kPa]	[%]	[%]
0	3.600	-	5.074 (±0.001)	3.645	-	1.25	-
20	3.653	178	5.117 (±0.009)	3.705	164	1.42	-7.54
40	3.710	171	5.161 (±0.018)	3.765	154	1.50	-10.02
60	3.769	164	5.213 (±0.018)	3.836	139	1.77	-14.85
80	3.832	157	5.269 (±0.075)	3.912	150	2.07	-5.00
100	3.899	152	5.316 (±0.013)	3.975	160	1.96	5.65
120	3.969	146	5.366 (±0.018)	4.044	135	1.88	-7.82
140	4.044	142	5.437 (±0.018)	4.135	129	2.27	-9.18
160	4.121	138	5.498 (±0.009)	4.215	153	2.28	10.72
180	4.202	135	5.549 (±0.009)	4.282	145	1.89	7.25
200	4.287	133	5.619 (±0.026)	4.372	139	2.00	4.19
220	4.374	132	5.680 (±0.035)	4.450	143	1.74	8.17
240	4.463	-	5.749 (±0.041)	4.538	-	1.68	-

P: Pressure, E_p: Peterson modulus ($E_p=\Delta P\ d_i/\Delta d_i$), d_o: Outer diameter, d_i: Inner diameter, e(x): the error of x between theory and experiment, Experimental outer diameter is given as Mean (±S.E.), Initial geometry: D_o=5.07, H=0.715.

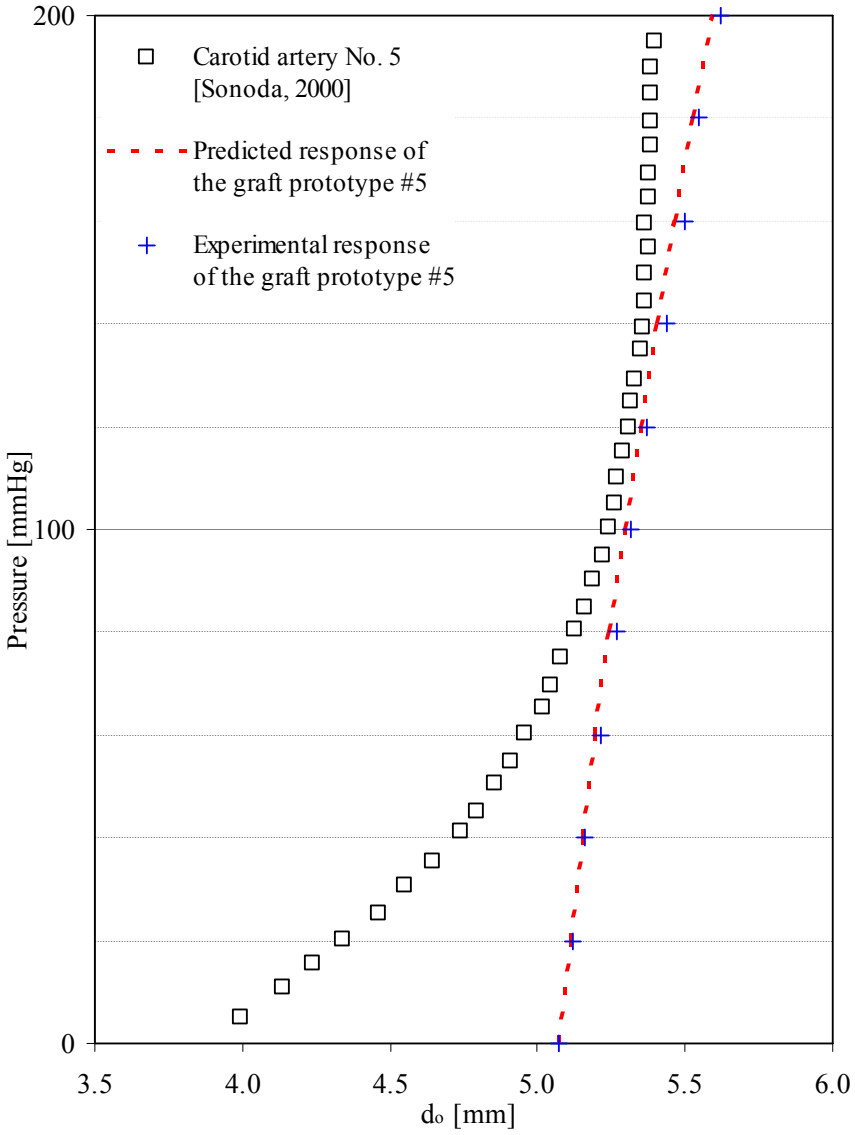

Figure 3.12: Predicted (dashed line) and experimental (+) pressure- diameter relationship of the graft prototype #5 and pressure- diameter relationship of the carotid artery No. 5 (□).

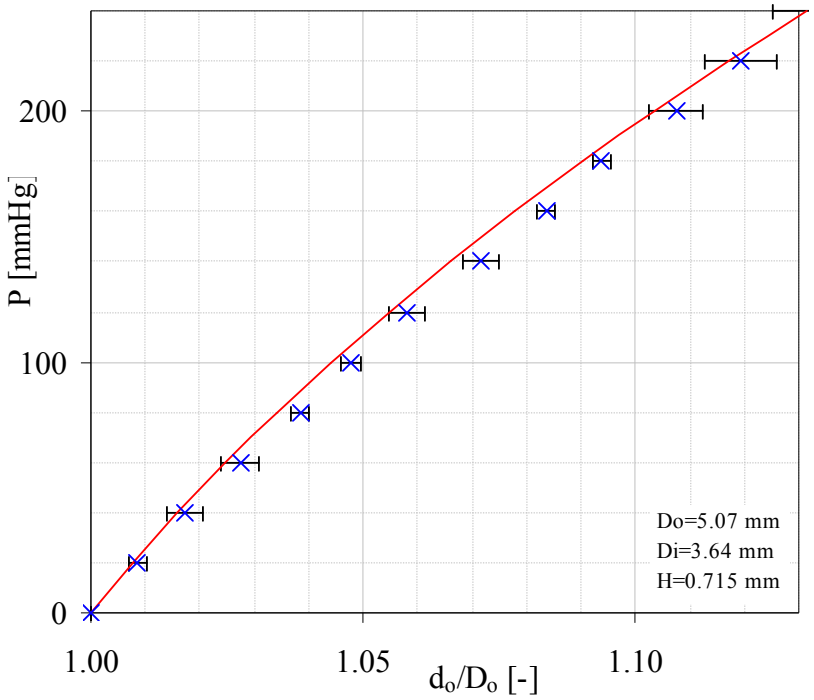

Figure 3.13: Predicted (solid line) and experimental (x) pressure-normalized diameter relationship of the prototype
Horizontal bars are the S.E. (n=3) of d_o/D_o.

The Pearson correlation between the theoretical and experimental pressure diameter curves is

$$r = 0.9999$$

Summarizing, the graft prototype #5 was fabricated within ±6% of specifications. The misfit between the predicted response of the prototype #5 and the canine carotid No. 5 [51] is within 5%. Therefore, the misfit between prototype #5 and the canine carotid No. 5 is about 10%.

If a graft is fabricated with the exact fabrication parameters, the misfit between the graft and the host artery can be reduced to 5%.

3.11 Burst pressure

Burst strength of the prototype #5

The burst pressure (Fig. 3.14) and burst stress are

$$P_{burst} = 744 mmHg$$

$$\sigma_{ult} = 690 kPa$$

Figure 3.14: Prototype #5 just before bursting

Burst strength of the other prototype

The theoretical burst pressure of the other prototype can be calculated assuming that their burst stresses are the same as the burst stress of the graft prototype. All prototypes appears to withstand theoretically the maximal pathologic blood pressure of 300mmHg, as shown in Table 3.13. As the tubes have identical material properties, the burst pressure depended primarily on the thickness, H.

Table 3.13: Other graft prototypes predicted burst pressure

	Prototype Graft #				
	1	2	3	4	6
P_{burst} [mmHg]	997	960	488	455	444

P_{burst}: Predicted burst pressure

CHAPTER 4

DISCUSSION

4.1 Summary of accomplishments

This work shows that we can design and build a mechanics matching graft. The fabricated graft prototype was within 6% of its specifications. Therefore, the overall process of design, fabrication and selection of a mechanics matching synthetic vascular graft was shown to be reliable and robust.

4.2 Comparison with ePTFE, Dacron, SVG, arteries

The comparison of mechanical responses between the designed human graft, prototype #5, arteries, saphenous vein, and current vascular grafts (5mm ID) is illustrated in Fig. 4.1. As prototype #5 was fabricated within 6% of its prediction, the same error is taken to calculate the possible range of fabricated dimensions of the human graft that best fit the LCCA (IOG_LCCA mechanical responses are given in Table 4.2). The current vascular grafts have mechanical responses that are far from the LCCA or RCCA responses (they are not compliant enough). The prototype #5 mechanical responses (Table 4.2) are the closest to an artery mechanical responses. The compliance of the prototype #5 is also close to the compliance of the CronoFlex™ (5 mm ID) graft, which is a more compliant synthetic graft in development [48].

Table 4.1: Comparison of mechanical responses at 100 mmHg of vascular grafts

	LCCA	IOG_LCCA	RCCA No.5	Prototype #5	SV	PU	PTE	ePTFE
d_i [mm]	4.32	4.32 ±0.13	5.24 (d_o)	5.3 ± 0.02 (d_o)	5.1	6.9	5.6	5.4
C [% mmHg 10^{-2}]	2.82	2.82 ±0.17	8.77	8.33	4.4	8.1	1.9	0.9

LCCA: Human Left Circumflex Coronary Artery [18], RCCA: Right Carotid Canine Artery No. 5 [51], SV: Saphenous vein, PU: Chronoflex™ (5 mm ID), PTE: Dacron™ (graft 5 mm ID), ePTFE: Gore-Tex™ (5mm ID) [53], IOG_LCCA: IOG for the LCCA host artery (designed value ± deviation from prediction).

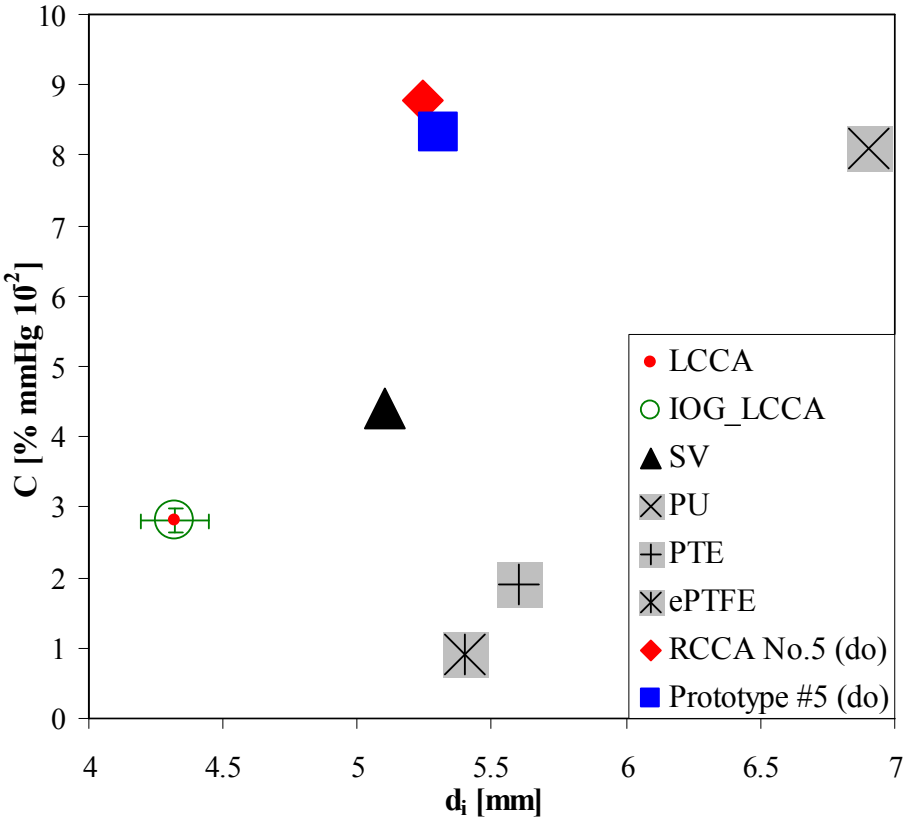

Figure 4.1: Compliance vs. diameter of SVG, vein, arteries, and prototype #5.
LAD: Human Left Anterior Descending Artery [16], SVG_LAD: Synhtetic vascular graft designed to fit the LAD (bars indicate the interval error of fabrication), SV: Saphenous vein, PU: Chronoflex™ (5 mm ID), PTE: Dacron™ (graft 5 mm ID), ePTFE: Gore-Tex™ (5mm ID) [53], RCCA No.5 (do): Right Carotid Canine Artery No. 5 (outer diameter) [51], Prototype #5 (do): Prototype #5 (outer diameter)

Many attempts to design a mechanics matching graft use Polyurethanes (PUs). Large-diameter vascular grafts fabricated from BioSpan (successor of Biomer) have been shown to retain their elastic characteristics long after repeated immersion in hot water, and they also exhibit better thromboresistance than materials such as PET and e-PTFE (http://www.polymertech.com/materials/biospan.html). The PU vascular grafts have faster neointimal cell migration and a thinner neointimal layer than ePTFE [23]. Many studies confirmed the excellent mechanical properties and favourable biofunctionality of these grafts, but only a few reports have been concerned with the chemical stability (oxidation) and the degradation (mineralization, environmental stress-cracking) of segmented PUs [31]. The biocompatibility or biostability of PU surfaces is still under debate [31]. Moreover, PU grafts performance and compliance are not well characterized due to the various composition of the PUs. [60].

Rather than seeking a functionally equivalent synthetics graft, some research groups try to mimic the host artery over the whole physiological range of pressure variation. The grafts are either coaxial synthetic tubes [51] or tissue engineered arterial grafts (TEAG). The coaxial synthetic tubes are difficult to manufacture and are still mechanically incompatible. The TEAGs use a bioresorbable material [17] as an initial conduit. The scaffolds are pre-seeded with living cells cultured in a bioreactor [34] and the growth of tissue is stimulated by chemical and mechanical conditioning [33, 50]. The difficulties of processing and controlling the cells growth are the main disadvantage of this method.

4.3 Limitation of approach

This first approach is limited by the need for materials with a SEF that are biocompatible, hydrophilic and easy to manufacture, The second approach requires a wider range of diameters, thickness as well as compliance to be sure to fit one individual. Problems related to those limitations are discussed in the following.

Design optimization theory

The mechanically equivalency assumption, formulated in the "one point criterion", states that the pressure diameter curves of the host artery and graft are tangent at the mean pressure. This assumption is reasonable because the graft and the host artery have mechanical responses that are almost linear in the physiological range of pressure. A graft that follows the criterion will reduce the discontinuity stress at the anastomotic sites. Therefore, no local stress analysis is needed. The thin wall tube assumption that considers the stresses uniformly distributed through the wall, is sufficient for tubes with deformed wall thickness inferior to 20% of the deformed radius, which is the case here. A thick wall tube assumption has a small (less than 5%) effect on the mechanical responses we are interested in. The constitutive formulation of the material uses an elastic model based on the strain energy function (SEF). Thus, the design optimization can be applied to all biomaterials whose SEF is known or can be identified by experimentation. The highly non-linear equations resulting from the design optimization problem are solved using an iterative floating-point arithmetic (fsolve in Maple). Note that an fsolve computation may fail to find a root even though one exists, in which case specifying appropriate range information may result in a successful computation (Waterloo Maple Inc.).

The "one point criterion" supposes the graft to be end-to-end anastomosed to the host artery. To design an end-to-side anastomosed graft, another criterion that best describes a reduced stress at the anastomotic sites should be considered. The local pick of stresses due to the suture wires is not taken into account. Because the thickness of the graft is almost the same as the host artery, this effect is supposed to be small at least in the radial direction. Moreover, the healing of the arterial tissue will create a continuous connection between the graft and the host artery that will progressively remove the load from the suture lines. The junction between the graft and the host artery may also be assured using glue or compliant stents to avoid the use of suture wires. In some cases (in the human model studied for instance), the thickness is too great and a stiffer material that will reduce the thickness should be considered to fabricate a suitable graft.

The mechanical approaches to studying the IH focus on the local wall stress distribution at the anastomotic sites typically uses finite element analysis [2, 5, 20, 29, 35, 39]. The finite element method allows one to define a precise geometry of the anastomotic sites [29, 39]. However, the non-linear behavior of the materials is often linearized to suit for solving with this approach [2, 29, 35, 39]. The suture wires' local stresses are rarely investigated [2], because the models become too complex. In any case, the model is difficult to set-up and needs simplifications to solve for both non-linear geometry and physics. Few groups [35, 51] propose a procedure to design a mechanics matching graft. They relate that their prostheses are still mechanically incompatible.

Selection of a graft

Design outcomes were found for both canine carotid and human coronary host arteries. The design outcomes for the canine arteries give thin wall grafts that can be

easily manufactured. A set of 6 grafts was built to cover the possible range of variation of the canine carotid host artery parameters.

Design outcomes were found for other arteries (small and large), but were not reported in this work. The host artery parameters must be measured on each patient to be able to select a patient specific graft. Today, the non-invasive measurement of the axial force is difficult. Hopefully, the design outcomes are almost not sensitive to the axial force parameter of the host artery, so that its value can be taken from the literature. Therefore, the host artery inner diameter at the diastolic, systolic and mean pressure and those respective pressures are sufficient to select a graft that best fits a patient. To be sure to find a graft that suits a given canine carotid host artery with an error less than 10% for both the diameter and compliance, a set of 21 grafts (3 different diameters and 7 different compliances) should be fabricated. Each time the error is reduced by two, the number of grafts increases by four. The success of finding a graft to best fit one individual determines the number of different grafts fabricated.

Current grafts are selected only to fit the mean diameter of the host artery [48]. The functional stiffness of the graft is not labeled and is not a criterion of selection of a graft.

Experimental setup

The experimental setup is the traditional "pressure-outer diameter" video measurement. It takes an important place in the design and validation of a mechanics matching graft. The local measurement of the outer diameter with a high resolution CCD camera remains the easiest setup to measure the pressure diameter relationship. The sensitivity obtained with the video measurement system was about $1.74 \cdot 10^{-2} mm / pixel$. The pressure resolution

was about 1 mmHg. The temperature of the bath containing the graft is set to 37°C before the first measurement. Longitudinal and radial marks are made before mounting the graft on the cannulas to verify the non-deformed state before inflation.

Data recorded with this experimental setup can be used to identify the SEF of materials which depends only on the first strain invariant, like elastomers (Polyurethanes, Silicon, PVA hydrogel) [3, 62]. To identify the SEF of more complex materials, the instrument should impose torsion on the sample in addition to stretching and inflation as described by Yang [59]. The limitations of the measurement were due to the roughness, and imperfections of the material, and the water environment. The data processing was time consuming because the acquisition was not automated. An automated digital image processing software (Montivision) was tried but produced data with noise due to the water environment. No control loop is used to keep the temperature constant at 37°C. At the end of the experiments the temperature is about 25°C (room temperature). However, the small Standard Deviations of the measurements indicate that the hydrogel is not subjected to large structural modifications between 25°C and 37°C. In any experimental setup, the sample placement is the key factor to make relevant measurements. A twisting or stretching of the tube during its placement might cause an undesired tube deformation. The longitudinal and radial marks allow the initial configuration of the sample to be checked before performing the inflation test.

Other measurement techniques (ultrasound, volume change measurement) [18, 6] are able to measure the inner and outer diameter at the same time. The advantage of these techniques is to give information about the compressibility of the material. In many cases, this information is not sought because the material considered is incompressible. In

this work, the incompressibility assumption of the material is reasonable because of the high water composition (>90%) of PVA hydrogel used. Then, the inner diameter is calculated assuming this incompressibility. The resolution of other measurement techniques (about 0.01 mm for an ultrasound system) is not higher than the video measurement with a high resolution CCD camera (about 0.017 mm) and is often more complicated to setup. The "change of volume" measurements are less accurate because they measure the diameter along the graft which is not a perfect cylinder during the inflation.

4.4 Need for in vivo test of IH

A set of grafts optimized for the canine carotid should be fabricated in order to test the hypothesis of this project in a canine model. By fabricating 21 grafts (equally distributed within the proposed range of fabrication), we should find always a graft with a misfit less than 10%. By implanting the best fitted graft at one carotid and a commercially available synthetic graft (control) at the other carotid, the patency of the graft could be compared. A graft with only a misfit of 10% should greatly increase its patency, because there is almost a linear correlation between the compliance mismatch and the low patency rate that is hypothesized [48].

Currently, ChronoFlex™ (segmented polyurethane) vascular grafts are human synthetic CABGs in development. Seven graft sizes were proposed as shown in Fig. 5.1. ChronoFlex vascular grafts (5 mm ID) were tested in animals. The grafts were implanted in dogs in a bilateral abdominal aorta to iliac artery position [52]. The error in the diameter was about 2.4% and 47% and the error in the functional stiffness about 38% and 77% when respectively compared to the canine lower abdominal aorta and external iliac.

Even if these errors are high, the patency of the graft was followed up over a period of 36 months. Therefore, a mechanics matching graft with a misfit of less than 10% (our case) may exhibit an improved long term patency (more than 36 months).

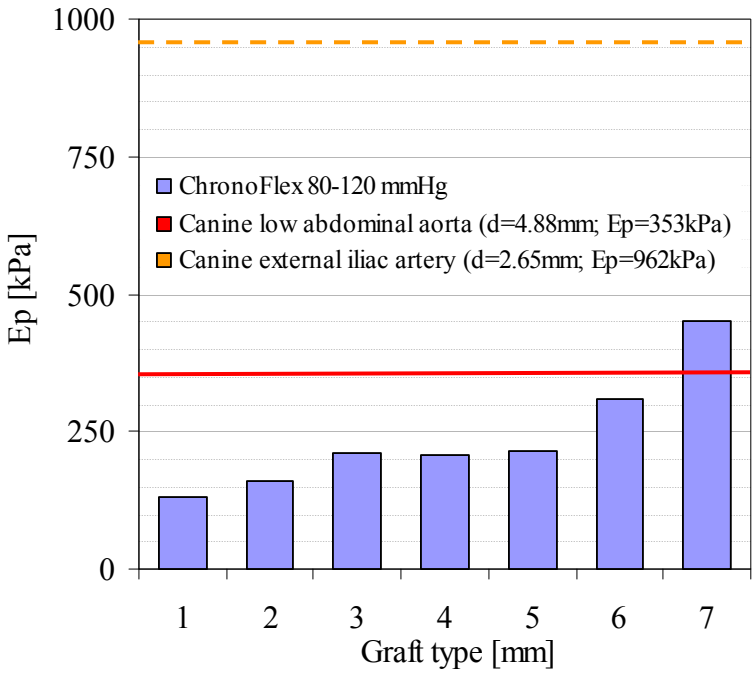

Figure 4.2: Functional stiffness of different types of ChronoFlex grafts and canine low abdominal aorta and external iliac artery [38, 48]

4.5 Clinical advantage

The clinical advantages are the following:

i. In optimistic expectations, the patency lifespan could be highly increased and could benefit the patient,

ii. The use of elastic materials gives better pulsatility than current SVG,

iii. The grafts are easy to manufacture when compared to other attempts to build compliant grafts,

iv. The grafts are off-the shelf.

4.6 Conclusions and recommendations

The hypothesis of this thesis is that a mechanics matching plus biocompatibility, hydrophilicity, and geometric matching can be designed and fabricated. It was shown that we can design and fabricate a mechanics matching graft according our criteria. The graft might be made of any material whose SEF is known or can be determined. This includes biomaterials such as elastomers (Polyuréthanes, Silicon, PVA hydrogel) or other rubber-like materials. PVA hydrogel was selected because its biocompatibility, non-thrombogenicity, elastic properties and flexibility in composition and processing are advantageous for vascular graft development. A prototype small diameter graft was fabricated to fit a given carotid host artery. The mechanical response of the prototype was close to its theoretical prediction and its strength withstands physiological pressure. Therefore, the overall process of design, fabrication, and selection of a mechanics matching graft appears to be robust and reliable. The mechanical matching grafts could reduce the intimal hyperplasia at the anastomic sites and enhance life of patients in the immediate future.

First, the expected long term patency of these mechanics matching grafts should be verified. Several graft prototypes should be tested in a canine model for thrombosis and intimal hyperplasia development. The overall procedure could be tested by fabricating a set of 21 canine carotid grafts, measuring the canine carotid artery by the non invasive technique, and selecting the prototype that best fit the dog. The echotracking

measurement technique is able to measure the thickness of the artery. A range of materials with different stiffness could be fabricated to give the choice of the thickness of the graft. The graft that best fits one given artery is then the one that minimizes the error between the diameter, compliance, and thickness between the host artery and the graft. A thickness matching may reduce any post operative stresses due to the suture wires.

Finally, another criterion to relate the mechanical equivalency of a graft end-to-side anastomosed to the host artery could be investigated. The set of 21 grafts is optimized for a canine model to select a graft with less than 10% misfit. This can not be transposed to the human model. More data on human coronary arteries should be collected to determine the range of fabrication parameters to be able to select an individual human coronary graft with a reduced misfit (<10%). The design optimization could be adapted to an end-to-side anastomosed graft. The mechanics matching criterion must then be changed. It is possible to predict the axisymetric deformation of a circular (elliptical) aperture in the wall of a cylinder by knowing its cross-sectional deformation. Therefore from the pressure- outer diameter relation of one given host artery, the geometrical dimensions and compliance of the circular aperture in the wall is deduced. The resulting diameter at mean pressure and compliance at mean pressure of the circular aperture constitute the new criteria. Then, the design optimization follows what has been described in this work.

APPENDIX A

"PREDICTED MECHANICAL RESPONSES OF PVA HYDROGEL GRAFTS" PROGRAM

```
#########################################################################
#                                Units                                  #
#########################################################################
# Pressure in [mmHg]
# Material constant a in [-]
# Material constant c in [kPa]
# Dimensions in [mm]
# Stresses in [kPa]
# Ep in [kPa]
# Fz in [g]
#########################################################################
#                            Inputs/Outputs                             #
#########################################################################

#Input: Pressure, Initial load and geometry, Material constant
#Output: Mechanical responses (d, Ep)

restart;

#########################################################################
#        Pressure at which you want to predict the mechanical responses #
#########################################################################
Pressure:=100:

#########################################################################
#                          Initial load and geometry                    #
#########################################################################
lambda1:=1.159609687;
Ri:=1.866683737:
H:=.3601869800:

#########################################################################
#                            Material Constants                         #
#########################################################################

a:=0.8502593:
c:=81.62497227:

#########################################################################
```

```
#                                SEF of the material                                #
#####################################################################################

I1:=l1^2+l2^2+1/(l1*l2)^2:
Phi:=a*(I1-3):
W:=(c/a)*(exp(Phi)-1):

#####################################################################################
#                                      Program                                      #
#####################################################################################

#Initial geometry
Do:=2*(Ri+H):
Dm:=Do-H:
Rm:=Dm/2:

#Deformed geometry
h:=H/(l1*l2):
ri:=Rm*l2-0.5*h:
rm:=Rm*l2:
ro:=Rm*l2+0.5*h:

#Material constitutive equations
e1:=(1/2)*(l1^2-1):
e2:=(1/2)*(l2^2-1):
dWde1:=diff(W,l1)*(diff(e1,l1))^(-1):
dWde2:=diff(W,l2)*(diff(e2,l2))^(-1):
s1:=l1^2*dWde1:
s2:=l2^2*dWde2:

#Peterson Modulus calculation
        #Differential definition
        P:=h*s2/ri:
        Epeterson1:=diff(P,l2)*(diff(ri,l2))^(-1)*ri:

        #Global definition
        DeltaP:=40:
        h1:=H/(l1*l2_1):
        h2:=H/(l1*l2_2):
        ri1:=Rm*l2_1-0.5*h1:
        ri2:=Rm*l2_2-0.5*h2:
        Epeterson2:=(DeltaP)*ri/(7.5*(ri2-ri1)):


#Deformed circumferential stretch numerical solving
l1:=lambda1:
```

```
        #For diastolic pressure (needed for Ep_global calculation)
        P1:=(Pressure+10^(-8)-DeltaP/2)/7.5:
        l2_1:=fsolve(s2=P1*ri/h,l2,0...5):

        #For systolic pressure (needed for Ep_global calculation)
        P2:=(Pressure+DeltaP/2)/7.5:
        l2_2:=fsolve(s2=P2*ri/h,l2,0...5):

        #For mean presssure
        P:=Pressure/7.5:
        l2:=fsolve(s2=P*ri/h,l2,0...5):

#Results
lambda2:=l2;
E1:=e1;
E2:=e2;
sigma1:=s1;
sigma2:=s2;
di:=2*ri;
dm:=2*rm;
d0:=2*ro;
Ep_differential:=Epeterson1;
if P1<0 then Ep_global:="No answer" else Ep_global:=Epeterson2 end if;
Fz:=evalf(Pi*(2*rm*h)*s1)/10;
```

APPENDIX B

”DESIGN OUTCOMES” PROGRAM

```
restart;

#########################################################################
#                                Units                                  #
#########################################################################
# Pressure in [mmHg]
# Material constant a in [-]
# Material constant c in [kPa]
# Dimensions in [mm]
# s1,s2 in [kPa]
# Epam in [kPa]
# Fam in [10xg]

#########################################################################
#                             Inputs/Outputs                            #
#########################################################################

#Input: Host artery parameters
#Output: Fabrications parameters

#########################################################################
#                          Host artery parameters                       #
#########################################################################

#Mean Pressure [mmHg]
Pm:=100:

#Inner radius @ mean pressure [mm]
riam:=4.114991320/2:

#Perterson modulus @ mean pressure [kPa]
Epam:=66.98591321:

#Axial force @ mean pressure [10xg]
Fam:=517.7299967:

#########################################################################
#                          Material Constants                           #
#########################################################################
```

```
a:=0.8502593:
c:=81.62497227:

#########################################################################
#                                SEF of the Material                    #
#########################################################################

I1:=l1^2+l2^2+1/(l1*l2)^2:
Phi:=a*(I1-3):
W:=(c/a)*(exp(Phi)-1):

#########################################################################
#                                Program                                #
#########################################################################

#Initial geometry
R:=Ri+H/2:

#Deformed geometry
r:=R*l2:
h:=H/(l1*l2):
ri:=r-h/2:

#Material constitutive equations
e1:=(1/2)*(l1^2-1):
e2:=(1/2)*(l2^2-1):
dWde1:=diff(W,l1)*(diff(e1,l1))^(-1):
dWde2:=diff(W,l2)*(diff(e2,l2))^(-1):
s1:=l1^2*dWde1:
s2:=l2^2*dWde2:

#Equilibrium equation
P:=h*s2/ri:

#"One point" criterion equation [(eq1)-(eq3)] and Equilibrim equation [Eq.(eq4)]
eq1:=ri-riam:
eq2:=diff(P,l2)*(diff(ri,l2))^(-1)*ri-Epam:
eq3:=s1*2*Pi*h*r-Fam:
eq4:=Pm/7.5*ri-h*s2:

#Numerical solving of the system of equations (Eqs. eq1-eq4)
sols:=fsolve({eq1,eq2,eq3,eq4},{l1=0.8..1.2,l2=0.8..1.2,H=0.1..8,Ri=1..15}):

#Save and display results
map( lhs, sols ):
assign(sols):
```

```
lambda1:=l1;
l2:=l2:
Ri:=Ri;
H:=H;
currentdir():
save lambda1,Ri,H,"Design_outcomes.txt";
```

APPENDIX C

"SELECTION OF THE BEST MANUFACTURED GRAFT FOR THE PATIENT" PROGRAM

```
#########################################################################
#                                Input/Output                           #
#########################################################################

#Input: Individual measurements
#Output: The best graft

restart;

#########################################################################
#                          Individual measurements                      #
#########################################################################

Pressure [mmHg]
        Diastolic Pressure
                Pd:=80:
        Mean Pressure
                Pm:=100:
        Systolic Pressure
                Ps:=120:

Inner Diameter [mm]
        @Diastolic Pressure
                diad:=3.929:
        @Mean Pressure
                diam:=4.115:
        @Systolic Pressure
                dias:=4.262:

            ###########################################################
              ########################################################
                ######################################################
                  ####################################################

#########################################################################
#                                Units                                  #
#########################################################################
# Pressure in [mmHg]
# Material constant a in [-]
# Material constant c in [kPa]
# H, Ri in [mm]
```

```
# s1, s2 in [kPa]
# Ep in [kPa]
# Fz in [g]

#########################################################################
#                        Individual Parameters Calculation              #
#########################################################################

#Functional stiffness of the HA of the patient [kPa]
Eap:=(Ps-Pd)*diam/(7.5*(dias-diad)):

#########################################################################
#                        Available manufactured grafts                  #
#########################################################################

number:=6;
Ri(1):=1.43:H(1):=0.79:Ep100(1):=200:
Ri(2):=1.74:H(2):=0.92:Ep100(2):=192:
Ri(3):=1.76:H(3):=0.44:Ep100(3):=98:
Ri(4):=1.81:H(4):=0.42:Ep100(4):=91:
Ri(5):=1.82:H(5):=0.72:Ep100(5):=150:
Ri(6):=2.17:H(6):=0.49:Ep100(6):=89:

#########################################################################
#                        Material Constants                             #
#########################################################################

a:=0.8502593:
c:=81.62497227:

#########################################################################
#                        Implantation stretch ratio                     #
#########################################################################

l1:=1:

#########################################################################
#                        Weighting factor of radius                     #
#########################################################################

w:=0.6:

#########################################################################
#                        Program                                        #
#########################################################################
```

```
for i from 1 to number do

unassign('I1');unassign('Phi');unassign('W');unassign('Do');
unassign('Dm');unassign('Rm');unassign('h');unassign('e2');
unassign('dWde2');unassign('s2');unassign('P');unassign('E');
unassign('l2');

#SEF
I1:=l1^2+l2^2+1/(l1*l2)^2:
Phi:=a*(I1-3):
W:=(c/a)*(exp(Phi)-1):

#Initial geometry
Do:=2*(Ri(i)+H(i)):
Dm:=Do-H(i):
Rm:=Dm/2:

#Deformed geometry
h:=H(i)/(l1*l2):
ri(i):=Rm*l2-0.5*h;

#Material constitutive equations
e2:=(1/2)*(l2^2-1):
dWde2:=diff(W,l2)*(diff(e2,l2))^(-1):
s2:=l2^2*dWde2:

#Peterson Modulus calculation
P:=h*s2/ri(i):
E:=diff(P,l2)*(diff(ri(i),l2))^(-1)*ri(i);

#Deformed circumferential stretch
P:=Pm/7.5:
l2:=fsolve(s2=P*ri(i)/h,l2,0...5):

#Save values in memory
di(i):=2*(Rm*l2-0.5*h);
Ep(i):=E;

#Calculation of the error
e[i]:=sqrt(w*((di(i)-diam)/diam)^2+(1-w)*((Ep(i)-Eap)/Eap)^2):

end do:

#Find the minimum between all e[i]
        #Define a procedure to find the minimum value of a list
        minimum:=proc(t,n)
```

```
        local i,m:
        m:=infinity:
            for i from 1 to n do
                if t[i]<m then m:=t[i] fi:
            od:
        RETURN(m):
    end:

    #Replace the indice of the best value by good
    for i from 1 to number do
        if e[i]=minimum(e,number) then good:=i fi:
    od:

#Plot the MG state at the patient's mean pressure
with(plots):
p:=[pointplot([diam,Eap],legend="HA",color=COLOR(RGB,0,0,0),symbol=circle,
symbolsize=12)]:
t:=[textplot([diam,Eap,`HA`],align={ABOVE,RIGHT},font=[HELVETICA, BOLD, 8],
color=COLOR(RGB,0,0,0))]:

for g from 1 to number do
  MG(g):=cat( "MG", g):

p:=[op(p),pointplot([di(g),Ep(g)],legend=MG(g),color=COLOR(HUE,g/number),symbol
=box,        symbolsize=12)]:
  t:=[op(t),textplot([di(g),Ep(g),MG(g)],align={ABOVE,RIGHT},font=[HELVETICA,
OBLIQUE, 8],        color=COLOR(HUE,g/number))]:
  points:=op(p);
  texts:=op(t);
od:
Titre:=cat("MGs and individual HA @", Pressure, "[mmHg]"):
display({points,texts},title=Titre,labels=[`di [mm]`,`Ep [mmHg]`],
labeldirections=[HORIZONTAL,VERTICAL]);

#Give the best graft in a sentence
cat(`The optimal graft for this patient is the Manufacture Graft # `,good, `, labelled :`);
[Ri(good),Ep100(good)];

#Calculate the Geometrical and Compliance Mismatch
cat(`[Geometrical,Compliance] mismatch in  [%]:`);
GM:=(di(good)-diam)/diam:CM:=(Ep(good)-Eap)/Eap:
[evalf[4](100*GM),evalf[4](100*CM)];

#Save results in "MG_best_fit.txt"
digood:=di(good):Epgood:=Ep(good):Rigood:=Ri(good):Ep100good:=Ep100(good):
currentdir():save good,Rigood,Ep100good,digood,Epgood,GM,CM,"MG_best_fit.txt";
```

REFERENCES

1. Abbott, W.M., Bouchier-Hayes, D.J., 1978, The role of mechanical properties in graft desing. Graft Material Vascular Surgery (Ed. Dardik H.), Chicago, Year Book Medical Publisher, 1978, 59-78.

2. Ballyk, P.D., Walsh, C., Butany, J., and Ojha, M., 1998, Compliance mismatch may promote graft artery intimal hyperplasia by altering suture-line stresses. J. Biomechanics, 31:229.237.

3. Beatty, M.F., 1987, Topics in finite elasticity: hyperelasticity of rubber, elastomers and biological tissues- with examples, Appl. Mech. Rev. 40: 1699-1734.

4. Benetos, A., Laurent, S., Hoeks, A., Boutouyrie, P., Safar, M., 1993, Arterial alterations with aging and high blood pressure: a noninvasive study of carotid and femoral arteries. Arterioscler Thromb;13:90–97.

5. Chandran, K.B., Gao, D., Han, G., Baraniewski, H., and Corson, J. D., 1992, Finite-element analysis of arterial anastomoses with vein, dacron and PTFE grafts. Med. Biol. Eng. Computing, 30:413.418.

6. Chin Quee, S., 2001. Design verification for tissue engineered vascular graft, M.S. Thesis, Georgia Institute of Technology.

7. Darling, R.C., Linton, R.R., 1972, "Durability of femoropopliteal reconstructions. Endarterectomy versus vein bypass graft", Am. J. Surg., 123: 472-479.

8. Depp, M.M., 1998, PVA cryogel optimization and diffusion studies, M.S. Thesis, Georgia Institute of Technology.

9. DeWeese, J.A., 1985, Anastomotic neointimal fibrous hyperplasia, In: V. M. Brenhard and J.B., Towne, eds., Complications in vascular surgery, 157—170. Orlando: Grune and Stratton.

10. Dobrin, P.B., 1998, Mechanics of End-to-End Artery-to-PTFE Graft Anastomoses, Ann Vasc Surg 1998;12:317-323.

11. Dobrin, P.B. , Littooy F. N. Endean E. D., 1989, Mechanical factors predisposing to intimal hyperplasia and medial thickening in autogenous vein grafts, Surgery, 105: 393-400.

12. Echave, V., Koornick, A.R., Haimov, M. and Jacobson, J. H., 1979, Intimai hperplasia as a complication of the use of the polytetraLtioroethylene graft for femoral-popliteal bypass, Surgery Vol. 86, pp.791-798.

13. Elshazly, T., 2004, Characterization of PVA hydrogels with regard to vascular graft development, M.S. Thesis, Georgia Institute of Technology.

14. Giron, F., Birtwell, W.S., Soroff, H.S. and Deterling, R.A. 1966, “Hemodynamic effects of pulsatile and nonpulsatile flow,” Arch. Surg., 93:802–810.

15. Glagov, S., Zarins, C.K., Giddens, D.P., Ku, D.N., 1989, "Mechanical factors in the pathogenesis, localization and evolution of atherosclerotic plaques" in Diseases of the Arterial Wall, (Springer-Verlag, N.Y.), pp. 217-239.

16. Gow B.S., Hadfield C.D., 1979, The elasticity of canine and human coronary arteries with references to postmortem changes. Circ. Res. 45:588-594.

17. Greisler, H., Endean, E., Klosak, J., Ellinger, J., Dennis, J., Buttle, K. and Kim, D., 1988, Polyglactin910/polydioxanone bicomponent totally resorbable vascular prostheses, J. Vasc. Surg., Vol. 7,pp. 697-705.

18. Hayash, K., Stergiopulos, N., Meister, J.-J., Greenwald, S., Rachev, A., 2001, Techniques in Determination of the Mechanical Properties and Constitutive Laws of Arterial Walls, Cardiovascular Techniques, 11, CRC Press.

19. He, G.W., 1999, Arterial Grafts for Coronary Artery Bypass Surgery, Springer-Vergag, Singapore.

20. Hofer, M., Rappitsch, G., Perktold, K., Trubel, W., Schima, H., 1996, Numerical study of wall mechanics and fluid dynamics in end-to-side anastomoses and correlation to intimal hyperplasia. J. Biomech., 29(10):1297.1308.

21. Imparato, A.M., Bracco, A., Kim, G.E., et al., 1972, Intimal and neointimal fibrous proliferation causing failure of arterial reconstructions. Surgery 72:1007.

22. Jarrell, B.E., Willams, S.K., Stokes, G. et al., 1986, Use of freshly isolated capillary endothelia 1 cells for the immediate establishment of a monolayer on a vascular graft at surgery, Surgery, 100: 392-399.

23. Jeschke, M.G., Hermanutz, V., Wolf, S.E., Köveker, G.B.., 1999, Polyurethane vascular prostheses decreases neointimal formation compared with expanded polytetrafluoroethylene. J Vasc Surg. Jan;29(1): 168-76.

24. Kroll, H.M., Hellums, D. J., Mclntire L., V. et al., 1996, Platelets and shear stress, Blood, 88(5): 1525-1541.

25. Ku, D. N., Braddon L. G., Wootton D. M., 1999, “Poly(vinyl alcohol) cryogel.”, US Patent no. 5981826.

26. Ku, D.N., Allen, R.C., 1995, Vascular Grafts, in The Biomedical Engineering Handbook (Bronzino, J.D., ed.), Boca Raton, FL, CRC Press, Inc., pp. 1871-1878.

27. Labarre, D., 1990, Heparin- like polymer surfaces: control of coagulation and complement activation by insoluble functionalized polymers, Int. 1 Artif. Organs, a3: 651-657.

28. Labarre, D., 2001, Improving blood compatability of polymeric surfaces, Trens Biomater. Artif. Organs, 15(1): 1-3.

29. Leuprecht, A., Perktold, K., Prosi, M., Berk, T., Trubel, W., and Schima, H., 2002, Numerical study of hemodynamics and wall mechancisin distal end-to-side anastomoses of bypass grafts. J. Biomechanics, 35:225.236.

30. Loop, F.D., Lytle, B.W., Cosgrove, D.M., Stewart, R.W., Goormastic, M., Williams, G.W., et al., 1986, Influence of the internal-mammary-artery graft on 10-year survival and other cardiac events. N Engl J Med 314:1-6:3484393.

31. Marois, Y., Guidoin, R., 2003, Biocompatibility of Polyurethanes, Eurekah Bioscience Collection.

32. Matsumoto, T., Itagaki, H. and Hayashi, K., 1994, FEM analysis of stress and deformation in vicinities of arterial graft anastomosis, J. Appl. Biomat., Vol. 5, pp.79—87.

33. Nerem, R.M. and Seliktar, D., 2001, Vascular Tissue Engineering, Annu. Rev. Biomed. Eng., Vol. 3, pp. 225-243.

34. Niklason, L.E., Gao, J., Abbott, W. M., Hirschi, K. K., Houser, S., Marini, R., Langer, R., 1999, Functional arteries grown in vitro. Science 284: 489-493.

35. Oijen C.H.G.A.van, 2003, Mechanics and design of fiber-reinforced vascular prostheses, PhD. Thesis, TU/e.

36. Ojha, M., 1994. “Wall shear stress temporal gradient and anastomotic intimal hyperplasia,” Circ. Res., 74: 1227–1231.

37. Okadome, K., Yukizane, T., Mii, S., Fukuda, A. and Sugimachi, K., 1989, “Correlations of long term results of femoropopliteal autogenous vein graft with shear stress variations: in situ or reversed graft,” J. Cardiovasc.Surg., 30: 932–935.

38. Patel, D.J., DeFreitas, F., Greenfield, J.C., Fry, D.L., 1963, Relationship of radius to pressure along the aorta in living dogs. J. Appl. Physiol. 18:1111-1117.

39. Perktold, K., Leuprecht, A., Prosi, M., Berk, T., Czerny, M., Trubel, W., and Schima, H., 2002, Fluid dynamics, wall mechanics and oxygen transfer in peripheral bypass anastomoses. Ann. Biomed. Eng., 30:447.460.

40. Peterson, L.H., Jensen, R.E., Parnell, J., 1960, Mechanical properties of arteries in vivo. Circ. Res.;8:622–39.

41. Pietrabissa; R., 1996, Biomateriali per organi articiali e protesi. Patron Editore.

42. Pomposelli, F.B. Jr., Arora, S., Gibbons, G.W., Frykberg, R., Smakowski, P., Campbell, D.R., Freeman, D.V. and LoGerfo, F.W., 1998, "Lower extremity arterial reconstruction in the very elderly: Successful outcome preserves not only the limb but also residential status and ambulatory function," J. Vasc. Surg., 28: 215–225.

43. Rachev; A., 2001, A Model of Arterial Adaptation to Alterations in Blood Flow, J. Elast., 61: 1-48.

44. Rachev, A, 2001, Remodeling of Arteries in Response to Changes in their Mechanical Environment, Biomechanics of soft tissue in cardiovascular systems, Springer-Verlag, New York.

45. Rachev, A., 2004, Constitutive Formulation of the Mechanical Properties of Synthetics Hydrogels, ASME.

46. Rittgers, S.E., Karayannacos, P.E. and Guy, J.F., 1978, "Velocity distribution and intimal proliferation in autogenous vein grafts in dogs," Circ. Res., 42: 792–801.

47. Roach, M.R. and Burton, A.C.,1957, The reason for the shape of the distensibility curves of arteries. Can. J. Biochem. Physiol. 35, 181–190.

48. Salacinski, H. J., Goldner, S., Giudiceandrea, A., Hamilton, G., Seifalian, A. M., 2001, The mechanical Behavior of Vascular Grafts: A Review, J. Biomat. Appl., V15: 241-277.

49. Salam, T.A., Lumsden, A.B., Suggs, W.D., Ku, D.N. "Low shear stress promotes intimal hyperplasia in a dose-response manner," J. Vasc. Investig. 2:1, 12-22, 1996.

50. Seliktar, D., Black, R.A., Vito, R. P., Nerem, R. M., 2000, Dynamic mechanical conditioning of collagen-gel blood vessel constructs induces remodeling in vitro. Ann Biomed Eng. 28(4):351-62.

51. Sonoda, H., Takamizawa, K., Nakayama, Y., Yasui, H., Matsuda, T., 2001, Small-diameter compliant arterial graft prosthesis: Design concept of coaxial double tubular graft and its fabrication, J Biomed Mater Res 55: 266–276.

52. Szycher; M.; Armini; A.; Bajgar; C., Lucas, A., 2002, Drug-Eluting Stents to Prevent Coronary Restenosis, IMX Paper v2.

53. Tai, N.R., Salacinski, H.J., Edwards, A., Hamilton, G., and Seifalian, A.M., 2000, Compliance properties of conduits used in vascular reconstitution, British Journal of Surgery, 87, 1516-1524.

54. Takamizawa, K., Hayashi, K., 1987, Strain energy density function and uniform strain hypothesis for arterial mechanics. J. Biomech. 20:7-17.

55. Tardy, Y., Meister, J.J., Perret, F., Brunner, H.R., and Arditi, M., 1991,Non-invasive estimate of the mechanical properties of peripheral arteries from ultrasonic and photoplethysmographic measurements. Clin. Phys. Physiol. Meas. 12: 39-54.

56. Tarry, C.W., Walsh, D.B., Birkmeyer, N.J. O., Fillinger, M.F., Zwolak, R.M. and Cronenwett, J.L., 1998, "Fate of the contralateral leg after infrainguinal bypass," J. Vasc. Surg., 27: 1039–1048.

57. Tozzi, P., 2001, Systolic axial artery length reduction. An overlooked phenomenon in vivo, Am J Physiol Heart Circ Physiol 280: H2300–H2305.

58. Walden, R., L'Italien, G. J., Megerman, J., Hasson, J. E., Abbott, W. M., 1980, Matched elastic properties and successful arterial grafting., Arch. Surg., 115,: 1166-1169.

59. Williams S., 1998, "Mechanical testing of a biomaterial for potential use as a vascular graft and auricular cartilage replacement", MS thesis, Georgia Institute of Technology.

60. Xue, L., Greisler, H.., 2003, Biomaterials in the development and future of vascular grafts. J. Vasc. Surg. Feb; 37(2): 472-80.

61. Yang, J., Liao, D., Zhao, J., and Gregersen, H., 2004, Shear Modulus of Elasticity of the Esophagus, Ann. Biomed. Eng.

62. Zidi, M. and Cheref, M., 2003, Mechanical analysis of a prototype of small diameter vascular prosthesis: numerical simulations, Computers in Biology and Medicine, 33:65-75.